BEST AVAILABLE IMAGES

Defective images within this document are accurate representations of the original documents submitted by the applicant.

Defects in the images may include (but are not limited to):

- BLACK BORDERS
- TEXT CUT OFF AT TOP, BOTTOM OR SIDES
- FADED TEXT
- ILLEGIBLE TEXT
- SKEWED/SLANTED IMAGES
- COLORED PHOTOS
- BLACK OR VERY BLACK AND WHITE DARK PHOTOS
- GRAY SCALE DOCUMENTS

IMAGES ARE BEST AVAILABLE COPY.

As rescanning documents *will not* correct images, please do not report the images to the Image Problem Mailbox.

REMARKS/ ARGUMENTS

The Final Office Action of March 11, 2004 has been carefully reviewed and this response addresses the Examiner's concerns.

Status of the Claims

Claims 1-3, 6-7, 10-12, 14-19, 66-67, 69-70 and 125 were pending in the application. Claims 119-124 are withdrawn from consideration.

In view of the examiner's earlier and present restriction requirements, applicants retains the right to present claims 119-124 in divisional applications.

Claims 1-3, 6-7, 10, 12, 14-19, 66-67 and 69-70 and 125 were rejected under 35 USC 102(b) as being anticipated by Bal et al. (*Anal. Chem.*, 1994, 66:3423-3430).

Claims 1-3, 6-7, 10-12, 14-19, 66-67, 69-70 and 125 were rejected under 35 U.S.C. §103(a)as being unpatentable over Bal et al. in view of Farmer et al. (J. Mass Spectrom., 1998. 3:697-704).

Claim 1 is amended to further describe the Applicants' invention.

Support in the Specification to Amendments to Independent Claim 1

The analyzing the sample by matrix-less light desorption/ionization mass spectroscopy, after the sample has been applied to the deposited continuous film l is supported by p. 23, lines 19-21 ("*The component of the present invention dealing with light (laser) desorption for mass spectrometry is a matrix-less laser desorption approach. It uses the deposited semiconductor films of Table 1.*"), p. 29, lines 12-14 ("*The proteins, peptides and ammonium citrate used to demonstrate matrix-less mass spectroscopy with the three film morphologies of Table 1 were obtained from Sigma and the trypsin was frozen, sequencing grade from Promega.*"), p.30, lines 16-17 and Fig. 4 ("*FIG. 4 typifies results from a continuous (void free) film.*"), p. 36, lines 1-2 ("*In light (laser) desorption using the matrix-less approach, rapid thermal heating of non-matrix substrates is what releases the molecules from the surface.*').

Claims 1-3, 6-7, 10, 12, 14-19, 66-67 and 69-70 and 125 were rejected under 35 USC 102(b) as being anticipated by Bal et al. (Anal. Chem., 1994, 66:3423-3430).

Applicants respectfully traverse these rejections for the reasons presented below.

In order to better understand the differences between the present invention and the Bal et al. paper it should be recognized that in the Applicants' invention the continuous films have optical properties and species adsorption properties essentially the same as the optical properties and the species adsorption properties of the continuous film bulk material and the sample is analyzed by matrix-less light desorption/ionization mass spectroscopy.

In comparison, as generally pointed out by the examiner, the Bal et al. paper discloses a method of analyzing protein by matrix-assisted laser desorption/ionization mass spectrometry (MALDI mass spectrometry) (Abstract; pg. 3423, left col., lines 1-6; pg. 3424, left col., line 45 to right col., line 17). The method comprises depositing a Nafion film by evaporation onto a stainless-steel probe (metal substrate) (pg. 3425, lines 13-27) and applying the sample directly onto the Nafion film after the deposition of the film (pg. 3425, left col., line 39 to right col., line 2). The Nafion film is a perfluorinated cation exchanger with sulfonic acid groups (carbon hydrogen mixture) and possesses a high surface activity and can selectively bind small cations and organic cations covalently (species adsorption/analyte adsorption) (pg. 3424, left col., line 45 to right col., line 17). Nafion in liquid form at a concentration of 5% in a mixture of 10% water and alcohols was used to apply to the stainless steel probe. The solution was air-dried to produce the film. (pg. 3425, left column, lines 13-17).

The following summary of the prior art description of the properties of Nafion is presented to support that at least one of the Applicants' claimed limitations, specifically, depositing a continuous film having optical properties and species adsorption properties essentially the same as the optical properties and the species adsorption properties of the continuous film bulk material, is not found in the Bal et al. paper.

"Nafion is initially produced in a salt form with its sulfonic acid groups neutralized." (Nafion: Physical and Chemical Properties available at http://www.permapure.com/newweb/Nafion%20properties.htm and provided in Appendix A).

As understood in the art, in the salt form, Nafion is not chemically active. Nafion can be "chemically activated by conversion of the salt form to the acid form." "Once activated, Nafion immediately begins to react with its surrounding environment. Moisture is absorbed and exchanged with the surroundings. Reactive organic gas components within the surrounding air may undergo chemical changes when exposed to the super-acid catalytic activity of Nafion. These organic gases may combine to form larger compounds that are liquid or solid in nature. Over time, these organic residues build up a deposit on the Nafion. The original color of the Nafion changes gradually from translucent to yellow, then brown, then even black." (Nafion: Physical and Chemical Properties available at http://www.permapure.com/newweb/Nafion%20properties.htm).

" [The] ionic properties of Nafion were created by adding sulfonic acid groups, a chemical with very strong ionic properties, into the bulk polymer matrix. Nafion is a super-acid catalyst. The sulfonic acid groups attached to the Teflon backbone within Nafion function as an extremely strong proton donor due to the stabilizing effect of the large polymer matrix attached to the sulfonic acid. Nafion is very selectively and highly permeable to water. The sulfonic acid groups in Nafion have a very high water-of-hydration, so they very efficiently absorb water. Interconnections between the sulfonic acid groups lead to very rapid transfer of water through the Nafion." (Nafion: Physical and Chemical Properties available at http://www.permapure.com/newweb/Nafion%20properties.htm).

Nafion films are originally amorphous but develop crystalline regions after a short period of time (a week). (M. Ludvigsson et al., J. Electrochem. Soc., 2000, 147: 1303-1305, provided in Appendix B, see pg. 1304, rt. column, second par.) the crystalline regions in Nafion become amorphous when wetted. (Ludvigsson, pg. 1305, left column, first paragraph). Since Nafion absorbs water, a Nafion film would have amorphous and crystalline regions depending on the water absorption. As the Nafion film absorbs water from the ambient, the film expands both vertically and laterally. (P.J. James et al., J. Material Sci., 2000, 35:5111-5119, provided in Appendix C, see pg. 5117, left column, line 5). Both AFM images and X-ray scattering indicate that clusters (clusters of ionic aggregation) form in the Nafion film and the clusters vary with water content, i.e. humidity (P.J. James, Figs. 3, 5, 6). Furthermore, it has also been shown that

the conductivity of the Nafion film varies with water content (Jeffrey B. Mecham, Ph. D. Thesis, Department of Chemistry, Virginia Polytechnic Institute and State University, 2001, provided in Appendix D, see pg. 84-87).

The Bal et al. paper is silent as to the optical properties. However, it is inherent that materials with different ratios of crystalline to amorphous volumes have different optical properties. (See for example, the use of crystalline to amorphous transitions in rewritable optical media such as CD-RW. See definition of phase change disk in Webopedia at http://www.webopedia.com/TERM/P/phase_change_disk.html a copy of which is provided in Appendix E). It is also inherent that materials with different conductivity have different optical properties since the materials interact differently with electromagnetic waves. Furthermore, it is also inherent that materials with different topography will scatter electromagnetic waves differently and will have different optical properties.

The Bal et al. paper discloses the use of a Nafion film in MALDI analysis of an analyte. In one example the analyte is a protein sample, The protein sample is obtained by electrophoretic analysis and HPLC (pg. 3424, right col., line 50 to pg. 3425, left col., line 12; pg. 3425, lines 30-39). The sample is mixed with a matrix (pg. 3424, right col., lines 37-49) for MALDI. The sample is analyzed by laser mass spectrometry (pg. 3424, right col., line 20-36).

Even further supporting Applicants' position stated above, presented below are details related to optical properties and adsorption properties of the Nation film.

Optical properties

The bulk material described in the Bal et al. paper is Nafion in liquid form at a concentration of 5% in a mixture of 10% water and alcohols. That a solution has different optical properties form those of the solute dissolved in the solvent when the solute is considered separately or any of the separate components follows from the classical work of Onsager, Kirkwood and others (see references in G, van der Zwan, Theories for the dielectric constant, available at www.chem.vu.nl/acas/Homepages/zwan/notes.html a copy of which is provided in Appendix F). Thus, the Nafion film does not have the same optical properties as the base solution at a concentration of 5% in a mixture of 10% water and alcohols. Furthermore, the

Nafion film will have different optical properties at different humidities since the Nafion film will have amorphous and crystalline regions depending on the water absorption according to Ludvigsson et al. while the Nafion solution at a concentration of 5% in a mixture of 10% water and alcohols would not have a variable reflectivity due to amorphous and crystalline regions.

Assume arguendo that the salt form (with its sulfonic acid groups neutralized) is considered the bulk material. In the salt form, Nafion is not active. The Nafion film has to be active for the film to serve as part of the active substrate for MALDI (Bal et al., pg. 3424, left column, last paragraph). The active film will have different optical properties at different humidities and organic residues will build up a deposit on the Nafion changing the color (optical property) gradually from translucent to yellow, then brown, then even black. Thus, the Nafion film does not have the same optical properties as the salt form.

Adsorption Properties

The bulk material described in the Bal et al. paper is Nafion in liquid form at a concentration of 5% in a mixture of 10% water and alcohols. In a solution the solvent molecules interact with the solute molecules in order to form loosely bonded aggregates. (C.W. Keenan, J. H. Wood, General College Chemistry, 3rd edition, 1966, p.236, provided in Appendix G). Thus, the sulfonic acid groups are not available to act as extremely strong proton donors and can not bind cations. In its active form, the sulfonic acid groups act as extremely strong proton donors and can bind small and large organic cations. Thus, the species adsorption properties of the Nafion film are not essentially the same as the species adsorption properties of the Nafion bulk material.

Assume arguendo that salt form (with its sulfonic acid groups neutralized) is considered the bulk material. With the sulfonic acid groups neutralized, the sulfonic acid groups are not available to act as extremely strong proton donors and can not bind cations. In its active form, the sulfonic acid groups act as extremely strong proton donors and can bind small and large organic cations. Thus, even under this assumption, the species adsorption properties of the Nafion film are not essentially the same as the species adsorption properties of the Nafion bulk material.

Thus, Bal et al do not teach depositing a continuous film having optical properties and species adsorption properties essentially the same as the optical properties and the species adsorption properties of the continuous film bulk material.

Furthermore, the Bal et al. paper discloses a method of analyzing protein by **matrix-assisted** laser desorption/ionization mass spectrometry (MALDI mass spectrometry) (Bal et al., Abstract; pg. 3423, left col., lines 1-6; pg. 3424, left col., line 45 to right col., line 17). As disclosed by Bal et al., the success of the MALDI experiments disclosed in the Bal et al. paper depends on the choice of the UV absorbing matrix (Bal et al. , p. 3423, rt. column, lines 5-6). In contrast, in the Applicants' claimed invention the sample is analyzed by matrix-less light desorption/ionization mass spectroscopy.

Thus, Bal et al. do not teach analyzing the sample by matrix-less light desorption/ionization mass spectroscopy, after the sample has been applied to the deposited continuous film.

To anticipate a claim a reference must teach every element of the claim. (MPEP § 2131). As pointed above, Bal et al do not teach depositing a continuous film having optical properties and species adsorption properties essentially the same as the optical properties and the species adsorption properties of the continuous film bulk material, and Bal et al also do not teach analyzing the sample by matrix-less light desorption/ionization mass spectroscopy, after the sample has been applied to the deposited continuous film.

Applicants respectfully assert that Claim 1 is not anticipated by the Bal et al paper and neither are any of the dependent claims. In addition, in view of the specific needs of Bal et al (as discussed above) and since Bal et al is lacking at least one patentable feature present in claim 1 and the dependent claims of the Applicants' invention, a modification of Bal et al under 35 U.S.C. §103 would also be inapplicable because such modifications are not taught by nor obvious under Bal et al, and if incorporated into Bal et al, would render Bal et al. inoperable for its intended functions.

Claims 1-3, 6-7, 10-12, 14-19, 66-67, 69-70 and 125 were rejected under 35 U.S.C. §103(a)as being unpatentable over Bal et al. in view of Farmer et al. (J. Mass Spectrom., 1998. 3:697-704).

As stated above, Bal et al. do not disclose depositing a continuous film having optical properties and species adsorption properties essentially the same as the optical properties and the species adsorption properties of the continuous film bulk material and Bal et al. also do not disclose analyzing the sample by matrix-less light desorption/ionization mass spectroscopy, after the sample has been applied to the deposited continuous film. Farmer et al. do not disclose depositing a continuous film having optical properties and species adsorption properties essentially the same as the optical properties and the species adsorption properties of the continuous film bulk material and Farmer et al. also do not disclose analyzing the sample by matrix-less light desorption/ionization mass spectroscopy, after the sample has been applied to the deposited continuous film. Therefore combining Bal et al. with Farmer cannot be used to establish nor disclose depositing a continuous film having optical properties and species adsorption properties essentially the same as the optical properties and the species adsorption properties of the continuous film bulk material and combining Bal et al. with Farmer also cannot be used to establish nor disclose analyzing the sample by matrix-less light desorption/ionization mass spectroscopy, after the sample has been applied to the deposited continuous film.

Under a 103 rejection, a prima facie case of obviousness of the invention is made in view of the scope and content of the prior art. In order to establish a *prima facie* case of obviousness, "there must be some suggestion or motivation, either in the references themselves or in the knowledge generally available to one of ordinary skill in the art, to modify the reference or to combine reference teachings. Second, there must be a reasonable expectation of success. Finally, the prior art reference (or references) must teach or suggest all of the claim limitations." MPEP § 2143.

Neither Bal nor Farmer separately or in combination teach all the patentable features of independent claim 1 and the dependent claims. In light thereof, Applicants respectfully traverse the 35 U.S.C. 103 rejection of the claims.

In conclusion, in view of the above remarks, Applicants respectfully request the Examiner find all claims, 1-3, 6-7, 10-12, 14-19, 66-67 and 69-70 and 125, allowable over the prior art and pass this case to issue.

Since the total number of claims is less than the number of claims already been paid for, no additional fees are required. However, if fees are required, they should be charged to Deposit Account No. 03-2410, Order No. 30626-101.

In accordance with Section 714.01 of the MPEP, the following information is presented in the event that a call may be deemed desirable by the Examiner:

ORLANDO LOPEZ (617) 854-4000

Dated: April 26, 2004

Respectfully submitted,
Stephen J. Fonash, et al., Applicants

By: 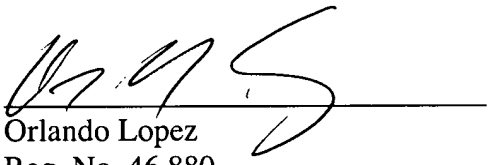
Orlando Lopez
Reg. No. 46,880
Agent for Applicants

Nafion: Physical and Chemical Properties

Background
Nafion®, was developed by Dr. Walther Grot at DuPont in the late 1960's by modifying Teflon®. Nafion was the first synthetic polymer ever developed with ionic properties, and it started an entirely new class of polymers called ionomers. These ionic properties of Nafion were created by adding sulfonic acid groups, a chemical with very strong ionic properties, into the bulk polymer matrix. Nafion combines the physical and chemical properties of its Teflon base material with ionic characteristics that give the final material the following properties:

a. Like Teflon, Nafion is extremely resistant to chemical attack. According to DuPont, only metallic alkali metals (sodium in particular) can attack Nafion directly under normal conditions of temperature and pressure. This means Nafion does not release fragments or degradation products into the surrounding medium.

b. Like Teflon, Nafion has relatively high working temperatures compared to many polymers. Nafion is used in some applications at temperatures up to 190° C.

c. Unlike Teflon, Nafion is highly ion-conductive. It functions as a cation exchange polymer.

d. Nafion is a super-acid catalyst. The sulfonic acid groups attached to the Teflon backbone within Nafion function as an extremely strong proton donor due to the stabilizing effect of the large polymer matrix attached to the sulfonic acid.

e. Nafion is very selectively and highly permeable to water. The sulfonic acid groups in Nafion have a very high water-of-hydration, so they very efficiently absorb water. Interconnections between the sulfonic acid groups lead to very rapid transfer of water through the Nafion.

Applications
These unusual properties are exploited in the four main applications of Nafion today.

1. Nafion is used to fabricate ion-exchange membranes used to produce chlorine gas and lye (sodium hydroxide) by the electrolysis of salt water.

2. Nafion is used to selectively dry or to humidify gases. The largest segment of this application involves drying or humidifying breath for anesthesia, respiratory care, or plethysmography, but many applications exist in the laboratory and in industrial use.

3. Nafion is used as the proton exchange membranes in polymer electrode fuel cells.

4. Nafion is used as a super-acid catalyst in the production of fine chemicals.

Physical Appearance

Nafion is initially produced in a salt form with its sulfonic acid groups neutralized. In this form, Nafion is thermoplastic (extrudable and formable using heat and pressure), but not chemically active. Once extruded into its final form (typically sheet or tubing), Nafion is chemically activated by conversion of the salt form to the acid form. At this stage, Nafion is a translucent plastic that is similar in appearance to Teflon, but clearer and less opalescent.

Once activated, Nafion immediately begins to react with its surrounding environment. Moisture is absorbed and exchanged with the surroundings. Reactive organic gas components within the surrounding air may undergo chemical changes when exposed to the super-acid catalytic activity of Nafion. These organic gases may combine to form larger compounds that are liquid or solid in nature. Over time, these organic residues build up a deposit on the Nafion. The original color of the Nafion changes gradually from translucent to yellow, then brown, then even black.

The chemical nature of the Nafion itself is not changed by this process. The Nafion is not directly attacked, and the Nafion is not degraded. Its properties of water permeability, ion-exchange, and acid catalysis are not directly affected.

For Nafion to transport water (dry or humidify gases), the water must be able to reach the active sites on the surface of the Nafion. In extreme cases, deposits of organic residues can build up on the Nafion to the point where the surface of the Nafion is sufficiently occluded to reduce its functionality. When this occurs, the discoloration of the Nafion is severe, black rather than merely yellow or brown. Even in these extreme cases, Nafion is still functional, it merely loses efficiency. Loss of a few percent of its total functionality due to partial occlusion means that a gradual decline in performance will be observed, not a catastrophic failure.

Under typical storage or operating conditions, Nafion will turn somewhat yellow within a year and brown within three to five years. Even after turning brown, the Nafion is still fully functional, and no loss of performance efficiency is likely to be observed.

These unwanted chemical reactions in the air surrounding Nafion are stimulated by exposure to light and to elevated temperatures. Storage in sealed bags in the dark will extend the pristine original appearance of Nafion.

The original clear appearance of Nafion can be restored by cleaning. Various cleaning solvents may be used if desired, usually non-polar solvents such as hexane. The most effective cleaning method (used by Perma Pure Inc. in its dryer service procedures) is to boil it in strong acid. Nafion is not damaged by these procedures, but the discolored surface residues are eliminated.

Go to top | Home | Who we are | Our Technology | Applications | Technical Notes | Products | FAQ
Int'l Distributors | What's new | Site Map | Contact us

Perma Pure LLC, P.O. Box 2105, 8 Executive Drive, Toms River, NJ 08754
(800) 337-3762, (732) 244-0010 Fax: (732) 244-8140

Journal of The Electrochemical Society, 147 (4) 1303-1305 (2000)
S0013-4651(99)06-021-8 CCC: $7.00 © The Electrochemical Society, Inc.

Crystallinity in Cast Nafion

M. Ludvigsson, J. Lindgren,* and J. Tegenfeldt*

The Ångström Laboratory, Inorganic Chemistry, Uppsala University, SE-751 21 Uppsala, Sweden

The performance of a polymer electrolyte fuel cell is critically dependent on the water uptake in the polymer electrolyte, usually Nafion. Nafion in solution is often painted onto the electrodes of the fuel cell. It is important that this cast Nafion film stay amorphous and not crystallize. Cast Nafion films, *ca.* 1 μm thick, crystallized on silicon plates when kept in air at room temperature for a long time. The films contain large crystalline regions ranging from 0.5 mm to several millimeters in size. X-ray diffraction (XRD) and Fourier transform infrared (FTIR) microspectroscopy have been used to investigate the crystalline and amorphous regions. The XRD shows two sharp peaks. One of the peaks is developed before the second one appears in the diffractogram, indicating that there might be two types of crystallizing processes. FTIR spectra of the amorphous and crystalline regions in the films show important differences. In the crystalline regions, the film contains the sulfonic acid at the end of the side chains; hence, the crystalline regions contain no water molecules. In the amorphous regions there is a complete proton transfer from the acid to the water molecules, and sulfonate groups are obtained.

Manuscript submitted June 2, 1999; revised manuscript received December 10, 1999.

Nafion™ is a perfluorosulfonic polymer membrane having exceptional chemical, thermal, and mechanical stability. It can act as a cation exchange membrane and it has found application as a separator in chlor-alkali cells. More recently, and due to its high proton conductivity, Nafion has attracted much interest as a polymer electrolyte membrane in polymer electrolyte fuel cells (PEFCs). Recent reviews summarize the applications as well as the structure and properties of perfluorinated membranes.[1,2] To enhance the performance of the PEFC, Nafion in solution is painted onto the electrode surfaces. Results from wide-angle X-ray diffraction (WAXS) studies are rather inconsistent and imply that there is either no crystallinity in Nafion membranes,[3] that they are partly crystalline,[4] or that crystallinity can be introduced in recast amorphous films by thermal treatment.[5] An electron microscope study suggests that crystalline Nafion has a linear zigzag structure just as polyethylene.[6] This polyethylene-like structure is also supported by an investigation of thermally treated recast Nafion.[7]

Our question was whether it would be possible to introduce crystallinity into Nafion with some sort of heavy ion irradiation. We decided on xenon ions. Cast Nafion films irradiated in vacuum by xenon ions were in fact observed to crystallize. Even though the films were exposed to different doses of ions, they crystallized in the same way. The size of the crystalline regions was 0.5-10 mm and thus easily observed. This attracted our attention and some further investigations on this material were made, as well as on films prepared without any irradiation.

Experimental

Thin films (*ca.* 1 μm thick) of Nafion (equiv wt 1100) were cast on single-crystal silicon windows from a solution of lower aliphatic alcohols and water, Fluka Chemika. For use in another experiment, in an ongoing project, the films were put in vacuum, 10^{-3} mbar, for approximately 10 h while they were irradiated with xenon ions. The irradiation was made on the cyclotron facility at the The Svedberg Laboratory, Uppsala University. Each film was exposed to between 1 and 100 ions/μm^2. The films were stored at room temperature in the laboratory for future investigations.

After some time, large crystalline regions, 0.5-10 mm, were formed in the films (Fig. 1). If a drop of water was added to the crystalline region of the Nafion film, it became amorphous immediately. Fourier transform infrared (FTIR) microspectroscopy (reflection mode) and X-ray diffraction (XRD) were used to investigate the amorphous and crystalline regions. Due to the size of the crystalline regions, the infrared beam could be focused on either crystalline or amorphous regions to record infrared spectra in open air.

Furthermore, in another ongoing project, reference spectra at different relative humidities (RH) were recorded.[8] This experiment included a cell where the desired RH and temperature could be achieved. In the experimental arrangement it was possible to achieve a state where $n = 1$ ($n = H_2O/SO_3^-$), *i.e.*, in vacuum at room temperature.[9] The $n = 0$ state was achieved in vacuum at an elevated temperature. A Nafion film saturated with $n = 14$ could be obtained in 100% RH.[10]

The infrared spectra were recorded on a Bio-Rad/Digilab FTS 45 FTIR spectrometer (equipped with a microscope) covering 400-4400 cm^{-1} with a resolution of 2 cm^{-1}. The X-ray diffractograms were recorded on a Siemens D5000 diffractometer with Cu Kα radiation.

Results and Discussion

In Fig. 2, the infrared spectra of the crystalline and amorphous regions of a xenon-irradiated Nafion film are shown together with spectra of Nafion films containing, 0, 1, and 14 water molecules per sulfonate group.[8] The symmetric stretching band of the SO_3^--group terminating the side chains of Nafion is situated at *ca.* 1060 cm^{-1}. In the top spectrum (a) of crystalline Nafion two bands at *ca.* 1400 and 910 cm^{-1} appear. These two bands correspond to the ν(S=O) and ν(S–OH) stretching modes of the SO_3H group. These two bands do not appear in the IR spectrum (b) of the amorphous region of an

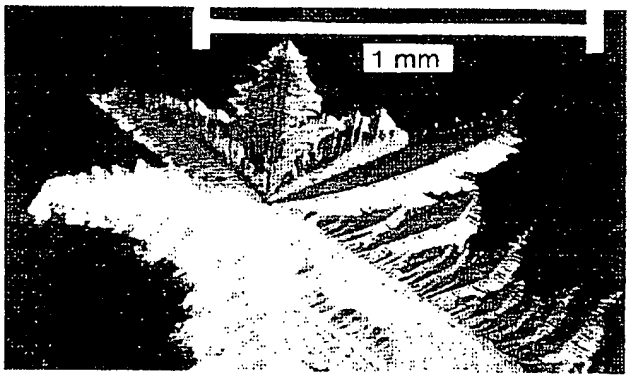

Figure 1. Crystallites in Nafion exposed to high vacuum and xenon ions.

* Electrochemical Society Active Member.
* E-mail: Jan.Lindgren@kemi.uu.se

S0013-4651(99)06-021-8 CCC: $7.00 © The Electrochemical Society, Inc.

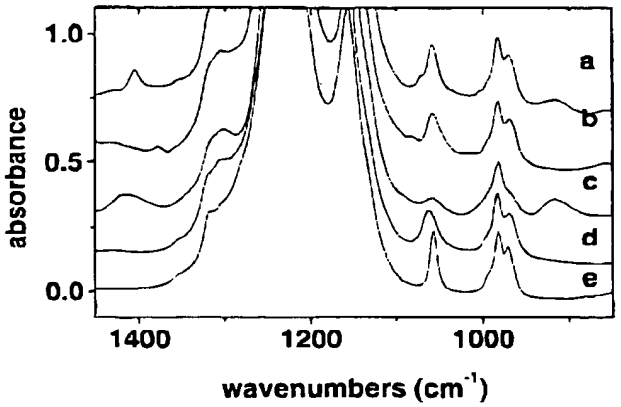

Figure 2. IR spectra of (a) the crystalline region and (b) the amorphous region of a crystalline Nafion film exposed to high vacuum and xenon ions and Nafion films containing (c) 0, (d) 1, and (e) 14 water molecules per sulfonate group.

irradiated film. They are present in a completely dried film as in spectrum (c) where there is no water at all. However, as soon as there is more than one water molecule per sulfonate group, the hydrogen is transferred to the water molecule, *i.e.*, the two bands are missing in spectrum (d) and (e).[8] This indicates that the side chains are terminated by SO_3H groups in the dry crystalline region and not by SO_3^- groups as in the amorphous region. Thus, the crystalline regions contain less water than the amorphous regions. This could be an additional reason why Nafion membranes absorb less water at elevated temperatures, provided that the Nafion membrane crystallizes partly at elevated temperatures.[11-13]

In the diffractograms (Fig. 3), the crystalline peaks of the Nafion film appear on top of the amorphous band. There are two broad amorphous features corresponding to d-spacings of 5.0 and 2.2 Å. In the upper diffractogram of a xenon irradiated Nafion there are four crystalline peaks, see Table I. In the lower diffractogram of a Nafion film kept at room temperature in the laboratory, only one peak is observed.

Porat *et al.* have made an electron microscope investigation of very thin Nafion films, 30-60 nm (compared to *ca.* 1 μm in the present study).[6] They found similarities with the electron microscopy data of polyethylene, see Table II. They concluded that the crystalline regions from the fluorocarbon backbone in their Nafion films had a linear zigzag structure just as polyethylene,[14] and not a twisted chain as polytetrafluoroethylene (PTFE).[15] The crystalline regions in the present study have spherulitic morphology. In general, spherulites grown from a bulk sample consist of lamellar crystalline plates of folded polymer chains which are perpendicular to the plane of growth, *i.e.*, the lamellae and the film itself (Fig. 4).[16-18] This is equivalent to a *c* axis oriented perpendicular to the plane of the Nafion film, and it can thus be assumed that we have the same preferred *c* axis orientation normal to the plane of the film as in the study by Porat *et al.* Thus, it is possible to calculate the lattice parameters *a* and *b* using the expression for an orthorhombic system: $d^{-2} = (h/a)^2 + (k/b)^2 + (l/c)^2$. The result is $a = 6.64 \pm 0.01$ Å and $b = 5.44 \pm 0.01$ Å (for Porat *et al.*, a = 7.49 Å and b = 5.02 Å). It is not possible to determine the lattice parameter c since part of the necessary information is missing. Our results thus indicate an orthorhombic cell but with different cell parameters from those of Porat *et al.* for Nafion and for polyethylene.

A sample of a cast Nafion film was kept in the laboratory at room temperature and under normal atmospheric conditions for an extended period of time to see if the crystallization is a spontaneous process or if the treatment with high vacuum and xenon ions is the cause. A diffractogram recorded directly after the film was cast shows only the broad amorphous features in Fig. 3. After a week, however, the strong peak at d = 2.72 Å appears in the diffractogram (Fig. 3), but 4 months later nothing else had happened and there was still only one crystalline peak. This may indicate that the full crystallization does not occur unless initiated, *e.g.*, by irradiation of xenon ions or by appli-

Table I. The d-spacings of the crystalline Nafion film in Fig. 3. Calculated values are obtained from a least-squares fit.

(*hkl*)	d-spacing (Å) Observed	d-spacing (Å) Calculated	Intensity
(110)	4.22	4.21	Strong
(200)	3.32	3.32	Weak
(020)	2.72	2.72	Strong
(220)	2.10	2.10	Weak

Table II. The d-spacings and suggested lattice parameters for crystalline polyethylene and Nafion.[12,6]

(*hkl*)	d-spacing (Å) PE	d-spacing (Å) Porat *et al.*
(110)	4.1	4.15
(200)	3.7	3.77
(020)	2.4	2.49
(310)	2.2	2.24

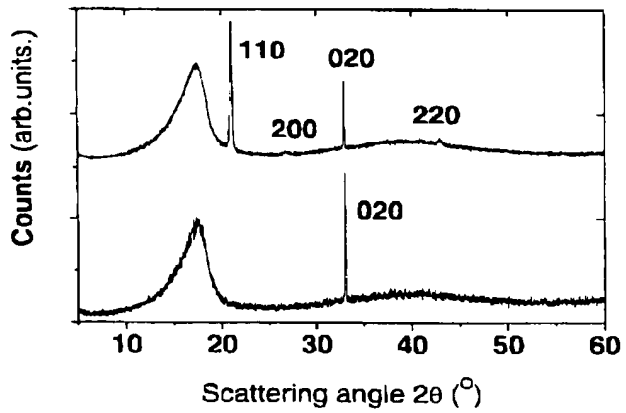

Figure 3. Diffractograms of 1 μm thick Nafion films: (top) film containing easily observable crystalline regions (exposed to high vacuum and xenon ion bombardment) and (bottom) film kept at room temperature and normal atmospheric conditions for 4 months.

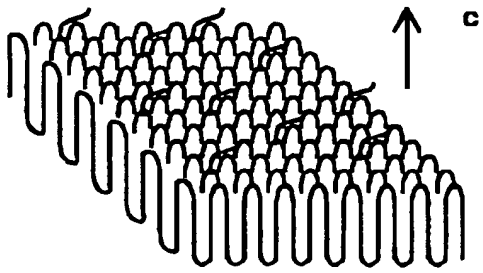

Figure 4. Schematic drawing of lamellar plates in the crystalline regions of spherulitic morphology.

Journal of The Electrochemical Society, 147 (4) 1303-1305 (2000)
S0013-4651(99)06-021-8 CCC: $7.00 © The Electrochemical Society, Inc.

cation of high vacuum and that some semicrystalline phase develops in a slow process in this film without the initiation. The exact coincidence of the single observed diffraction peak from the nonirradiated sample with the (020) peak from the irradiated sample would imply an ordering in one dimension in the *b* direction of the same type in both samples. The fact that the crystalline region became amorphous when wetted raises the question whether the irradiated polymer is crystalline because it is dried out or dehydrated because it is crystalline? Since only some regions of the Nafion films are crystalline and large amorphous areas are observed, we think that the latter statement is true. Otherwise the films ought to have crystallized completely. The introduction of these crystalline regions will probably not be of any harm in a fuel-cell application because they have been forced there with the help of xenon ion bombardment in high vacuum. Nevertheless, if they would appear in a dried-out membrane in an operating fuel cell, they are reverted to amorphous regions as soon as it is hydrated again. The silicon substrates seem to have no direct effect on the crystalline regions, since no preferred orientation can be found on any of the substrates.

Conclusions

In this work we used XRD and IR spectroscopy to study the crystalline phase of cast Nafion films. The earlier reported polyethylene-like orthorhombic structure of thin Nafion films is not supported by our results that indicate an orthorhombic structure with different cell parameters. There is, unfortunately, not enough information in the results from the XRD for a conclusion regarding the exact chain conformation or packing at present. Nevertheless, the IR spectra imply that the crystalline regions of the Nafion films contain less water than the amorphous regions.

Acknowledgments

This work has been supported by grants from the Swedish Natural Science Research Council (NFR), which is hereby gratefully acknowledged.

Uppsala University assisted in meeting the publication costs of this article.

References

1. C. Heitner-Wirguin, *J. Membr. Sci.*, **120**, 1 (1996).
2. S. Gottesfeld and T. A. Zawodzinski, *Advances in Electrochemical Science and Engineering*, Vol. 5, p. 197, John Wiley & Sons, New York (1997).
3. S. C. Yeo and A. Eisenberg, *J. Appl. Polym. Sci.*, **21**, 875 (1977).
4. T. D. Gierke, G. E. Munn, and F. C. Wilson, *J. Polym. Sci.*, **19**, 1687 (1981).
5. R. B. Moore and C. R. Martin, *Macromolecules*, **21**, 1334 (1988).
6. Z. Porat, J. R. Fryer, M. Huxham, and J. Rubinstein, *J. Phys. Chem.*, **99**, 4767 (1995).
7. G. Gebel, P. Aldebert, and M. Pineri, *Macromolecules*, **20**, 1435 (1987).
8. M. Ludvigsson, J. Lindgren, and J. Tegenfeldt, *Electrochim. Acta*, **45**, 2267 (2000).
9. N. J. Bunce, S. J. Sondheimer, and C. C. Fyfe, *Macromolecules*, **19**, 333 (1986).
10. T. A. Zawodzinski, Jr. C. Derouin, S. Radzinski, R. J. Sherman, V. T. Smith, T. E. Springer, and S. Gottesfeld, *J. Electrochem. Soc.*, **140**, 1041 (1993).
11. K. Broka and P. Ekdunge, *J. Appl. Electrochem.*, **27**, 117, (1997).
12. J. T. Hinatsu, M. Mizuhata, and H. Takenaka, *J. Electrochem. Soc.*, **141**, 1493 (1994).
13. P. C. Rieke and N. E. Vanderborgh, *J. Membr. Sci.*, **32**, 313 (1987).
14. J. F. Revol and R. S. J. Manley, *J. Mater. Sci. Lett.*, **24**, 249 (1986).
15. H. Chanzy, T. Folda, D. Gardner, and J. F. Revol, *J. Mater. Sci. Lett.*, **5**, 1045 (1986).
16. Y. Fujiwara, *J. Appl. Polym. Sci.*, **4**, 10 (1960).
17. E. J. Roche, R. S. Stein, and E. L. Thomas, *J. Polym. Sci., Polym. Phys. Ed.*, **18**, 1145 (1980).
18. J. D. Hoffman, G. T. Davis, and J. I. Lauritzen, Jr., in *Treatise on Solid State Chemistry*, Vol. 3, *Crystalline and Noncrystalline Solids*, N. B. Hannay, Chap. 7, Plenum, New York (1976).

JOURNAL OF MATERIALS SCIENCE 35 (2000) 5111–5119

Hydration of Nafion® studied by AFM and X-ray scattering

P. J. JAMES, J. A. ELLIOTT*, T. J. McMASTER
University of Bristol, H.H. Wills Physics Laboratory, Tyndall Avenue, Bristol, BS8 1TL, UK
J. M. NEWTON, A. M. S. ELLIOTT
National Power Innogy, Harwell International Business Centre, Harwell, Didcot, OX11 0QA, UK
S. HANNA‡, M. J. MILES
University of Bristol, H.H. Wills Physics Laboratory, Tyndall Avenue, Bristol, BS8 1TL, UK
E-mail: s.hanna@bristol.ac.uk

Nafion® is a commercially available perfluorosulphonate cation exchange membrane commonly used as a perm-selective separator in chlor-alkali electrolysers and as the electrolyte in solid polymer fuel cells. This usage arises because of its high mechanical, thermal and chemical stability coupled with its high conductivity and ionic selectivity, which depend strongly on the water content. The membrane was therefore studied in different states of hydration with two complementary techniques: atomic force microscopy (AFM) and small angle X-ray scattering (SAXS) combined with a maximum entropy (MaxEnt) reconstruction. Tapping mode phase imaging was successfully used to identify the hydrophobic and hydrophilic regions of Nafion. The images support the MaxEnt interpretation of a cluster model of ionic aggregation, with spacings between individual clusters ranging from 3 to 5 nm, aggregating to form cluster agglomerates with sizes from 5 to 30 nm. Both techniques indicate that the number density of ionic clusters changes as a function of water content, and this explains why the bulk volumetric swelling in water is observed to be significantly less than the swelling inferred from scattering measurements.

1. Introduction

Nafion® is a commercially available perfluorosulphonate cation exchange membrane (CEM) manufactured by E I du Pont de Nemours & Co. Inc. It is commonly used as a permselective separator in chlor-alkali electrolysers [1, 2] and as the electrolyte in solid polymer fuel cells (SPFC). Perfluorosulphonate cation exchange membranes are used in these applications because of their high ionic conductivity and their high mechanical, thermal and chemical stability. Structurally, Nafion consists of a hydrophobic tetrafluoroethylene (TFE) backbone with pendant side chains of perfluorinated vinyl ethers terminated by ion-exchange groups. The chemical structure of Nafion is shown in Fig. 1. The ion content can be varied by changing the ratio of the two components.

Other perfluorosulphonate cation exchange membranes with similar structures have also been developed by the Asahi Chemical Company (Aciplex®) and the Asahi Glass Company (Flemion®). The Dow Chemical Company also developed a material with a shorter side-chain than those of Nafion and the other perfluorosulphonates [3].

The ionic conductivity in perfluorosulphonate membranes is important since it should be as high as possible to minimize ohmic losses in chlor-alkali electrolysers and to maintain high output power densities in fuel cell applications. The membrane conductivity is strongly influenced by the water content [4]. Water management is also an important problem for efficient SPFC operation to avoid flooding of the gas diffusion electrodes. A number of factors affect the water content including the cation form, ion exchange capacity of the membrane and equivalent weight (EW). The ion content is usually expressed in terms of the equivalent weight of the polymer. The equivalent weight is defined as the weight of dry polymer in grams containing one mole of exchange sites. The desired equivalent weight is achieved by varying the ratio of vinyl ether monomer to TFE. The useful range of equivalent weights is from 600–1500 g per mole, between the solubility and percolation limits. The industrial applications of Nafion have

* *Present Address*: Department of Materials Science and Metallurgy, University of Cambridge, Pembroke Street, CB2 3QZ, UK.
‡ Author to whom all correspondence should be addressed.

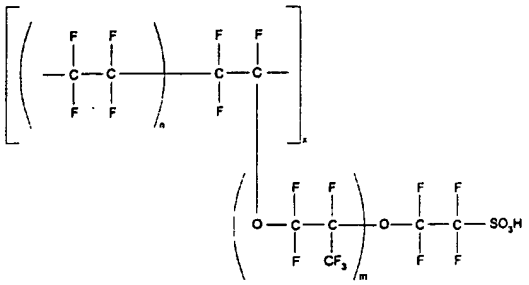

$C_{(2n+3m+4)}F_{(4n+6m+7)}O_{(m+4)}SH$

Figure 1 The structural repeat of Nafion.

prompted considerable research effort summarised by Eisenberg and Yeager in 1982 [5] and more recently by Tant *et al.* in 1997 [3].

Perfluorosulphonate polymers typically have ordered structures in which the hydrophilic end groups aggregate within a hydrophobic matrix composed of the fluorocarbon backbone of the polymer. The density contrast between the ionic aggregates and the matrix gives rise to scattering of X-rays [6–9] and neutrons [5]. The diffraction patterns show a broad ring reflection, the so-called 'cluster' reflection, with a peak position of 3.5–5.5 nm, together with a scattering upturn at low angles. Many different structural models have been proposed to explain these features, and they can be divided into two main groups. The first type are the interparticle models, such as the two-phase model [5, 10] and the lamellar model [5, 11], in which the scattering is produced by the interference between ionic aggregates. The second are the intraparticle models, such as the core-shell model [5, 12, 13], in which the scattering is due to fine structure within an individual ionic aggregate.

There have been a number of electron microscopy studies of Nafion [14, 15] which support the cluster model of phase separation, although the size scale of the structures observed did not correspond directly with those detected by scattering studies. The Cluster-Network model [5, 16] postulates a large scale organisation of clusters with transient connective tubes which are in constant flux. A fully-reversible dynamic reorganisation of the clusters is proposed to occur on rehydration. Positron annihilation spectroscopy has also been used to study different cation forms of Nafion membranes by measuring the free volume. These studies [17–19] found that the formation and expansion of clusters is always associated with a change in free-volume structure resulting in smaller free-volume holes.

There have been two recent studies undertaken using scanning probe microscopy (SPM) [20, 21], to investigate the structure of Nafion in differing states of hydration. A number of swelling studies have been carried out on Nafion [22, 23] using a wide variety of solvents with some remarkable results, including a swelling of 360% with tributylphosphate (TBP) as used by Lehmani *et al.* in their SPM study [21]. Nafion has proved to be a suitable sample for other forms of SPM including scanning tunnelling microscopy (STM) and scanning electrochemical microscopy (SECM) [24, 25]. Fan and Bard [24] studied a spin-coated Nafion film using SECM and found a domain-like structure, consisting of circular structures, 1–2 nm in diameter made up from a conductive central zone surrounded by a less conductive region.

Since many of the useful properties of Nafion membranes depend strongly on the water content, studies in different states of hydration using the two complementary techniques of atomic force microscopy (AFM) and small angle X-ray scattering (SAXS), might be informative. The difference in probe-specimen adhesion between the hydrophobic backbone and hydrophilic side group regions of Nafion offers the possibility of observing the spatial distribution of these two regions at the surface of the polymer using tapping mode phase imaging. Assuming that these are representative of the bulk, then the number density and average cluster size can be deduced as a function of water content, and the results compared with those from SAXS experiments.

2. Experimental method

2.1. Variation of the mass of Nafion with humidity

The uptake of water in Nafion membranes has been studied as a function of environmental humidity using a dynamic vapour sorption study (DVS) [26]. The sample was suspended in a 0% RH environment and weighed. The humidity was increased in steps using different saturated salt solutions, the sample was allowed to equilibrate and then weighed, the process was then repeated. A graph of percentage mass gain versus humidity was plotted from the data. Given that the equivalent weight of the sample and the theoretical weight are known, the average number of water molecules per sulphonic acid group can be calculated at 0% RH, by comparing the theoretical weight to the measured value. If it is assumed that all of the water is incorporated into the hydrophilic regions, a graph of average number of water molecules per sulphonic acid group can be plotted over the full range of humidities.

2.2. Sample preparation

All of the experiments were carried out using the most commonly used form of Nafion, 115H^+, which has the following physical properties; a nominal equivalent weight of 1100 (actually 1070) and thickness of 5 thousandths of an inch (~127 μm).

The membrane will readily rehydrate if left exposed to a high relative humidity environment [27]. Careless handling can result in the membrane ion-exchanging from the acid (H^+) to a salt form (e.g. Na^+ or K^+). All samples were therefore routinely prepared by refluxing with a 50/50 mixture by volume of concentrated nitric acid and de-ionized water, then de-ionized water alone, to ensure that the membrane is in the H^+ form and free from any chemical impurities.

2.3. Small-angle X-ray scattering

Two dimensional, point collimated SAXS data were collected using nickel-filtered Cu K_α radiation on a flat plate Rigaku-Denki camera, with a typical sample to

film distance of around 250 mm. The X-ray generator was an Elliott GX21 rotating anode generator. The films were scanned in transmission using an Optronics P2000 drum densitometer. The resulting images were converted to 8-bit binary files, with a pixel dimension of 100×100 μm. The low-angle limit due to beam divergence was approximately 0.026 nm^{-1}, which corresponds to a maximum discernible size for features in real space of around 40 nm. The diffraction patterns were corrected for Lorentz-polarisation effects and sample absorption.

Previous studies of SAXS from hydrated ionomer membranes used heat-sealed polymer bags to enclose the samples during exposure [6, 7]. This method was found to be unsatisfactory for quantitative work due to fluctuations in the environmental humidity level during the long periods (up to 24 hours) required to collect the SAXS data. An alternative approach, based on the controlled humidification of air using concentrated salt solutions, was adopted [28].

2.4. Maximum entropy method

A full account of the maximum entropy (MaxEnt) method used to interpret SAXS data has already been published [29], and only a summary will be presented here. The aim of the MaxEnt technique is to reconstruct a two dimensional charge density map which is a good fit to the observed scattering data. The MaxEnt criterion is required in order to resolve the inherent ambiguity in this fitting process due to the absence of phase information in the experimental data. Since there are many charge distributions which can give rise to identical diffraction patterns, we select the one with the highest entropy for a given goodness-of-fit. Of course, there is no guarantee that this model will necessarily be stereochemically or thermodynamically realistic, but if a reasonable structural interpretation can be found then we can be sure that this it is the most statistically likely interpretation which is consistent with the scattering data. In this way, the MaxEnt method is superior to other approaches which assume *a priori* a structural model. The algorithm used to carry out the reconstruction process is based on the 'Cambridge Algorithm' [30].

2.5. Atomic force microscopy

There are two principal modes of atomic force microscopy (AFM) [31] operation: contact mode and tapping mode. In contact mode, the tip remains in close contact with the sample, operating within the repulsive regime. In tapping mode, the cantilever is oscillated near to its resonant frequency, above the surface, only contacting the surface briefly during each cycle of its oscillation. Tapping mode is therefore more suitable for imaging delicate samples owing to the lower lateral forces and has been applied to many polymer systems [32–35]. It also has the added advantage of being able to obtain phase images as well as topographical data. Tapping mode phase imaging is a relatively new AFM technique, and it can differentiate between areas with different properties regardless of their topographical nature [36–42]. The phase angle is defined as the phase lag of the cantilever oscillation relative to the signal sent to the piezo driving the cantilever. Its value depends on the energy dissipated in the tapping interaction of probe and specimen [43, 44].

Circular samples 10 mm in diameter were mounted on magnetic stainless steel stubs, placed in the Digital Instruments Extended Multimode AFM and imaged in tapping mode with silicon cantilevers in order to provide topographic and corresponding phase images. The membrane and microscope were placed in a purpose-built environmental chamber to control the humidity and the samples were dehydrated overnight. A variety of techniques was employed to reduce the humidity including silica gel, phosphorus pentoxide, a liquid nitrogen cold finger and dry nitrogen gas. A humidity minimum of $(0.8 \pm 2.0)\%$ was obtained using nitrogen gas passed through molecular sieve material. The sample was then imaged and allowed to rehydrate slowly to room humidity $(34 \pm 2)\%$ over the course of 12 hours whilst being continuously imaged, and the humidity recorded.

2.6. Cluster counting algorithm

Phase images from the beginning and end of the rehydration sequence were analysed with the aid of a cluster counting algorithm [28, 45]. The 256×256 images were exported, cropped, saved as eight-bit data and then converted to binary. A series of thresholds from 0 to 256 was then applied to all the data points in the image; if the point was equal to or greater than the threshold value it was set to one (white), and, if not, it was set to zero (black). A cluster is defined as an isolated group of white pixels. The number of unique clusters, total area of clusters and average cluster area was then calculated for each threshold. The number of clusters at each threshold value was plotted for the two humidity extremes. The same algorithm was also used to analyse the MaxEnt reconstructions of the SAXS data acquired at ambient and 100% relative humidity.

3. Results and discussion

3.1. Variation of the mass of Nafion with humidity

Analysis of the DVS results is more revealing than previous studies [27]. In addition to a graph of percentage mass change against humidity (Fig. 2i), a graph of the ratio of water molecules to sulphonic acid groups against humidity (and not just the additional number) can be plotted (Fig. 2ii). This has been calculated using a theoretical dry mass for Nafion and by assuming that the EW is 1070. The difference in mass between the theoretical dry mass and that at 0% RH is the amount of water bound to the sulphonic acid groups. The average number of water molecules per sulphonic acid group at 0% RH was found to be 1.55. In the same regime as that used for the AFM data, in the humidity range of $(0–50) \pm 2\%$, on average an additional water molecule was added to each sulphonic acid group for an increase in RH of $14 \pm 2\%$. At higher humidities this becomes much more rapid and the assumption that all of the water is incorporated into the hydrophilic regions become less valid as water will start to condense on all regions of the membrane.

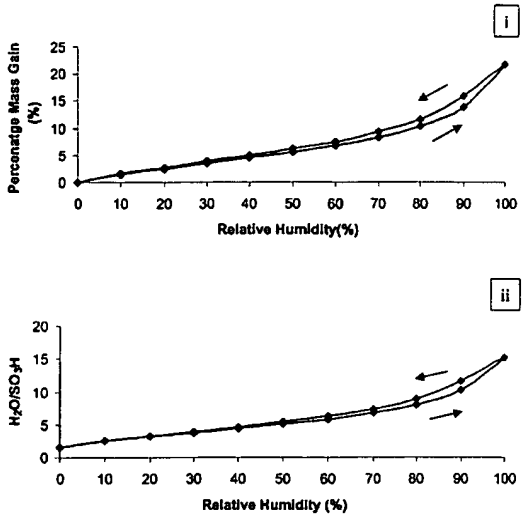

Figure 2 Percentage mass gain (i) and Number of addition water molecules per sulphonic acid group (ii) against relative humidity for Nafion 115 H^+. The relative humidity was cycled from to 0 to 100% and back again.

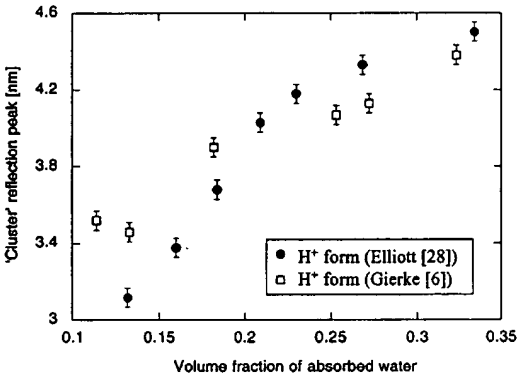

Figure 3 Peak position of the 'cluster' reflection from Nafion 115 H^+ membrane as a function of the volume fraction of absorbed water.

3.2. Small-angle X-ray scattering

The variation in the peak position of the 'cluster' reflection in the SAXS from a Nafion 115 H^+ membrane as a function of the volume fraction of absorbed water is shown in Fig. 3, along with the data published by Gierke *et al.* [6] for comparison. There are no values below a volume fraction of 0.1 as it was not possible to detect the 'cluster' reflection at such low water contents due to lack of electron density contrast. The dependence of the peak position on water content is predicted by the type of scattering model which is used to interpret the data. If the 'cluster' reflection were due to the coherence of intercluster spacings [5, 10], or the incoherent sum of interlamellar spacings [5, 11] then it might be expected that the increase in peak position would be directly proportional to the volume of absorbed water. However, if the reflection were produced by the scattering from individual three dimensional clusters models [5, 12, 13] then its spacing should vary with the cube root of the water volume. In fact, neither of these two simple behaviours occurs.

In order to explain the observed swelling behaviour, it is instructive to consider a MaxEnt interpretation of the scattering data. Fig. 4 shows MaxEnt reconstructions from membranes under ambient and 100% RH conditions. The MaxEnt reconstructions should be interpreted as 2-dimensional projections of the electron density distributions within a representative volume of membrane. Regions of low electron density appear light grey or white, while regions of high electron density appear dark grey or black. The absolute electron density range in each case is scaled to fit the grey-scale. The reconstructions are not unique, belonging to a large set of possible maximum entropy solutions, all of which are capable of reproducing the experimental data subject to the usual errors associated with X-ray counting statistics. However, the region of membrane represented in the reconstructions is sufficiently large that it is able to reproduce a wide range of structural variation within a single electron density map.

Both MaxEnt reconstructions contain fragmented regions of low charge density with a broad range of sizes. There is an increase in electron density contrast between these regions and the background, along with a coarsening of the size distribution from Fig. 4i (ambient) to Fig. 4ii (100% RH). In order to make the physical interpretation of these features clear, the reconstructions were spatially filtered to separate the small scale structures associated with the 'cluster' reflection from the large scale structures associated with the scattering upturn. The filtering was performed by windowing out the unwanted regions of the diffraction patterns, prior to MaxEnt reconstruction. The high spatial frequency images, shown in Fig. 4iii and iv for ambient and 100% RH respectively, both contain collections of point-like scatterers. However, as the water content is increased from Fig. 4iii to Fig 4iv, the spacing between the scatterers increases, and their number density decreases. It is the coherence of the spacings between the scatterers that is responsible for the 'cluster' reflection, and this interpretation is borne out by reconstructions from highly oriented samples [45]. We therefore identify the point-like scatterers as being individual ionic clusters.

The low spatial frequency images, shown in Fig. 4v and vi, show large scale structures which are composed of agglomerates of the clusters identified in the high frequency images. Although the agglomerates do not swell appreciably with increasing water content, the electron density contrast between these features and the polymer matrix increases noticeably due to the difference in density between the water and fluorocarbon phases. The shape of these cluster agglomerates, which is responsible for the form of the low angle upturn in the SAXS pattern, is related to the spatial coherence of the clusters. We therefore predict an intimate relation between the form of the upturn and the degree of arcing of the 'cluster' reflection. If the MaxEnt interpretation of the SAXS data is correct, then it should not be possible to see an arced 'cluster' reflection unless the low angle upturn is also anisotropic.

Assuming the MaxEnt interpretation is correct, then it is useful to calculate the relative number density of ionic clusters in Fig. 4iii and iv and relate this to the discrepancy between the bulk swelling of the membrane

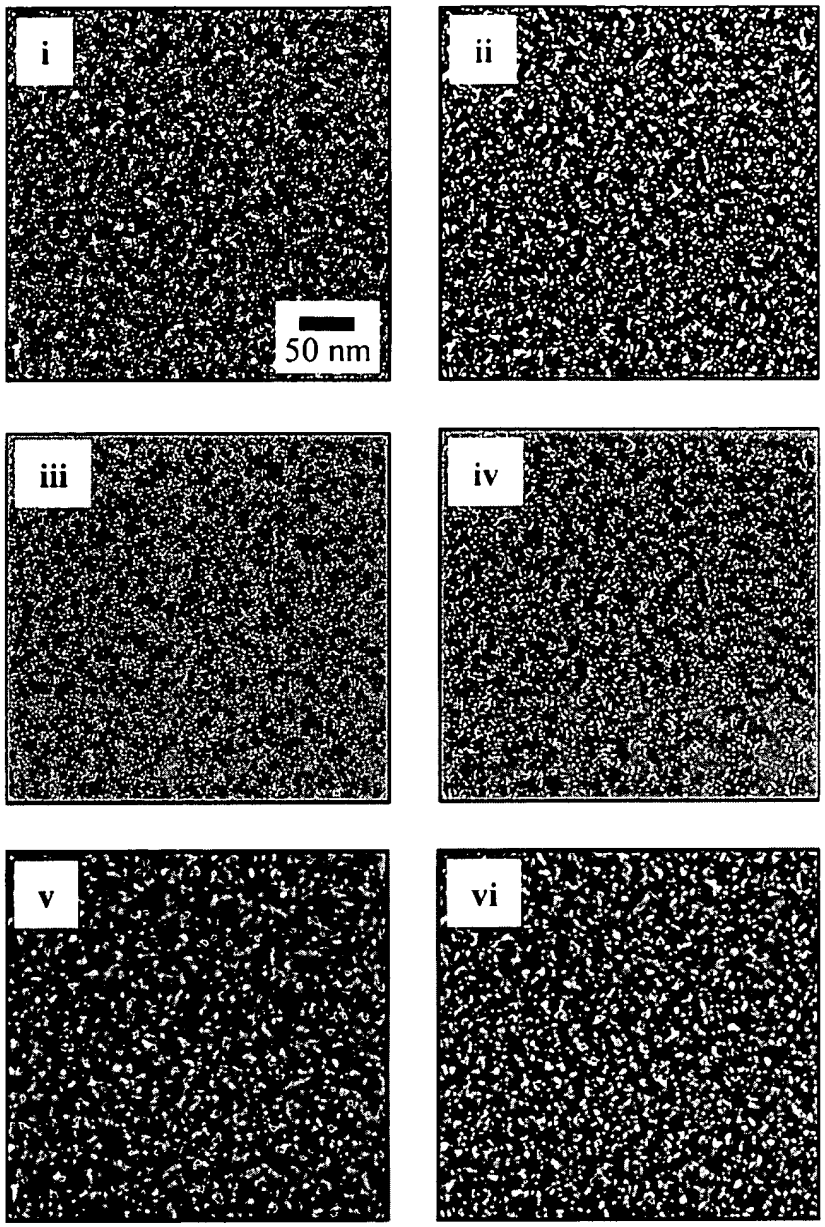

Figure 4 MaxEnt reconstruction of SAXS data from Nafion 115 H^+ membrane: (i) ambient humidity and (ii) 100% RH. The reconstructions have been high pass filtered in (iii) and (iv) and low pass filtered in (v) and (vi).

and the swelling which is inferred from the increase in the peak position of the 'cluster' reflection. Although the mean lateral intercluster separation increased by 44.1%, the overall lateral expansion of the membrane is expected to be significantly less than this due to a decrease in the number density of clusters. Unfortunately, it is difficult to predict the resultant macroscopic swelling quantitatively, because the electron density distributions are a 2-dimensional representation of 3-dimensional space. It is also possible that systematic changes in the spatial ordering of the clusters on swelling need to be incorporated into the model. Nevertheless, the mechanism described is qualitatively appealing and has been derived with the use of only very general *a priori* hypotheses, i.e.: (i) the use of a MaxEnt electron density distribution, (ii) the legitimacy of spatial filtering and (iii) the definition of a 'cluster' as an isolated agglomerate of pixels.

Although the redistribution of exchange groups was first predicted by the Marx infinite paracrystalline model [10] it is significant that this phenomenon can be inferred directly from the small angle X-ray data. In addition, there is also evidence for such a redistribution from phase contrast atomic force microscopy as discussed in the following section.

3.3. Atomic force microscopy

Six 1 μm phase images from a sequence of 56 images of 1070EW Nafion obtained over a range of humidities from (9–34) $\pm$ 2% are shown in Fig. 5i–vi. The phase

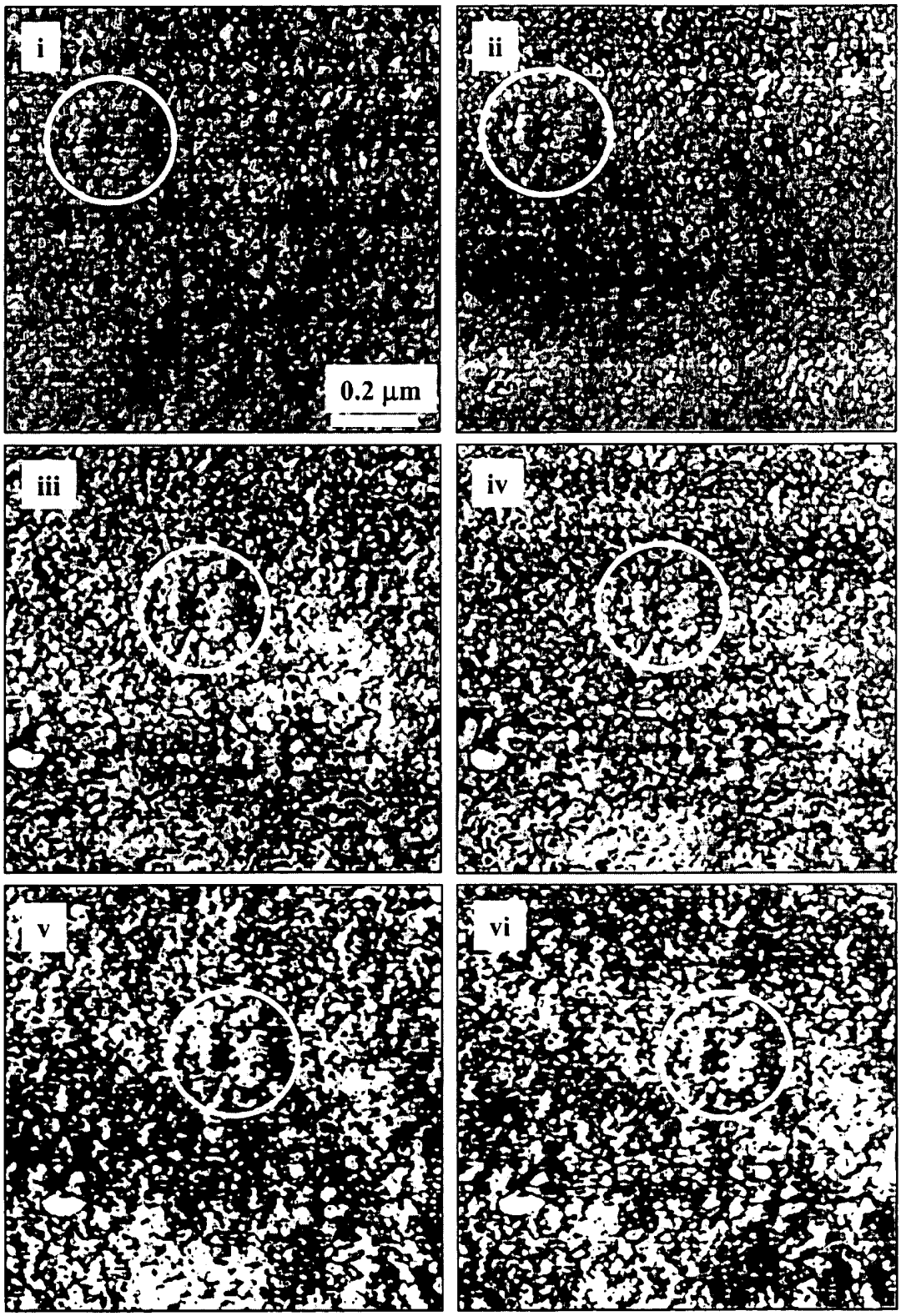

Figure 5 Six 1 μm tapping mode phase images of the same area of Nafion at relative humidities of (i) 9, (ii) 13, (iii) 19, (iv) 23, (v) 28 & (vi) 33 ± 2% (Z scale = 30°).

contrast between the hydrophilic sulphonic acid groups and the hydrophobic regions increases with humidity due to preferential sorption of water to the hydrophilic regions. It is very difficult to monitor the same area as the membrane expands both vertically and laterally. The same feature has been circled in each of the images to aid comparison and to illustrate the drift to the right which occurred throughout the series.

Cluster-like structures with a diameter of 5–30 nm are clearly visible, particularly in the phase images. These structures do not always correspond to features in the height image. Features at the same height can have a different phase signal and vice versa, indicating minimal topographic coupling. This is consistent with the earlier AFM studies [20, 21]. Chomakova-Haefke *et al.* [20], produced samples by evaporating a dilute solution of Nafion on to gold-sputtered cover slips. They were found to have a fibril network structure, which became more ordered as the membrane swelled. Lehmani *et al.* [21], imaged commercially available nominally 1100 EW Nafion 117. It was dehydrated in a vacuum oven at 80 °C and was first imaged "dry", then swollen with de-ionized water, and finally swollen with TBP. A super-structure of spherical domains with an average diameter of 45 nm containing 11 nm grains was found. According to the section analysis of the microstructure, the interstitial regions have a mean thickness of 5 nm, which may correspond to the cluster size.

The corresponding topography images from the beginning and end of the rehydration sequence are shown in Fig. 6i and ii respectively. The same area has been circled in both images demonstrating the ability to image the same area whilst following a dynamic process. There is no appreciable change between the two images, therefore any topographic coupling in the phase images remains constant and is not responsible for the increase in phase contrast.

Cluster counting analysis of the phase images from the beginning and end of the rehydration sequence is shown in Fig. 7i and ii, respectively, and tabulated in Table I. The sharp peak in Fig. 7i implies that all of the clusters have a similar phase angle and therefore energy loss at lower humidities. At higher humidities as shown in Fig. 7ii, the peak has moved to higher thresholds as the average energy loss has increased; the peak has also broadened significantly as the clusters have a wider range of energy losses. The average cluster area of between 134 and 158 nm^2 is consistent with the images shown in Fig. 5, where clusters have a range of linear dimensions between 5 and 30 nm (or

TABLE I The number of clusters, total percentage area of cluster and average cluster size for 1 μm wide phase images of Nafion at (9 & 34) ±2% relative humidity

Humidity ±2%	9	34
Number of Cluster	1415	1118
Total Percentage Cluster Area	18.9	17.6
Average Cluster Area (nm^2)	134	158

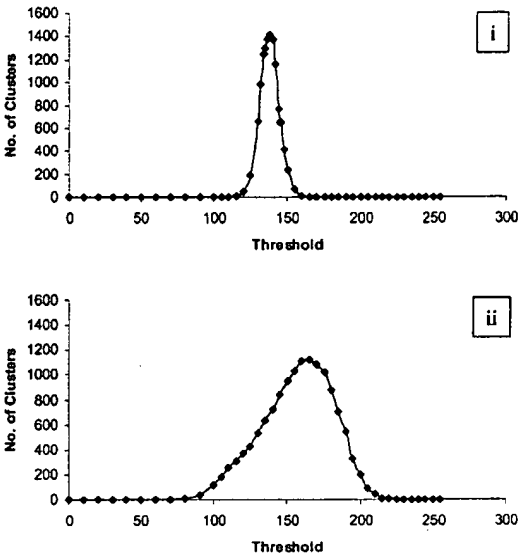

Figure 7 A graph of number of clusters against threshold value for the two humidity extremes of 9 & 34 ± 2%.

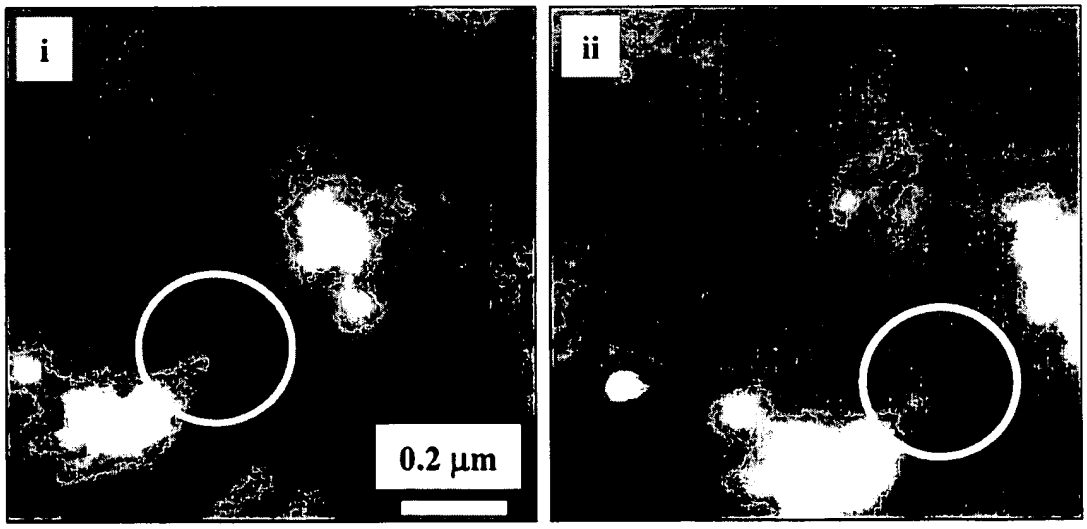

Figure 6 Topography images corresponding to those in Fig. 5i and vi for the humidity extremes of 9 & 34 ±2%. (Z scale = 50 nm).

approximate areas of 25 to 900 nm^2). This is significantly larger than the individual clusters which give rise to the 'cluster' reflection, but of comparable size to the cluster agglomerates.

The decreasing number of clusters and corresponding increase in average cluster size with humidity is consistent with the X-ray diffraction results described in the previous section and implies a cluster rearrangement similar to that proposed by Hsu & Gierke [16]. The percentage of the surface covered by clusters at 34 and 9% humidities, is 17.6 and 18.9% respectively. The larger percentage area at lower humidities can easily be explained by tip broadening effects, whereby a greater number of small features can appear to have disproportionately larger area than fewer larger features. This is considerably larger than a value of 7.6% calculated assuming: that the membrane is homogeneous and dry, that the mass of SO_3H is 81.1 g and the equivalent weight of the membrane to be 1070 (i.e. $(81.1/1070) \times 100$). However, the membrane is not dry and will have incorporated water preferentially into the hydrophilic clusters which will have swollen, the surface may not be representative of the bulk and the sulphonic acid group composition is 8% by mass, but not by volume.

4. Conclusions

The average number of water molecules per sulphonic acid group in Nafion 115 at 0%RH was found to be 1.55. If it is assumed that all of the additional water is incorporated into the hydrophilic regions as the humidity increased then in the approximately linear region between $(0–50) \pm 2\%$ RH an increase of $14 \pm 2\%$ in RH resulted in one additional water molecule per sulphonic acid group.

The most statistically likely structural model compatible with the MaxEnt reconstruction of the small angle X-ray scattering (SAXS) data is an interparticle model in which point-like ionic clusters aggregate to form higher order agglomerates.

Tapping mode phase imaging was successfully used to identify the hydrophobic and hydrophilic regions of Nafion perfluorosulphonate cation exchange membranes. Since there is often little correlation between the topography and phase images, it is a useful tool for identifying and mapping regions with different properties, irrespective of their topographical nature. The images support the MaxEnt interpretion of a cluster model of ionic aggregation, with spacings between individual clusters ranging from 3 to 5 nm, aggregating to form cluster agglomerates with sizes from 5 to 30 nm.

The phase images also showed that the number of clusters decreased and the average cluster size increased with increasing humidity. This is consistent with the interpretation of the MaxEnt charge distributions, and is reminiscent of the redistribution of ionic material between clusters proposed in the cluster-network model [16]. The change in number density of ionic clusters as a function of water content explains why the bulk volumetric swelling in water is observed to be significantly less than the swelling inferred from scattering measurements.

It is significant that the same conclusions were obtained using two different experimental techniques operating over complementary ranges of relative humidity. This indicates that the swelling and redistribution of ionic clusters in Nafion is a dynamic process occurring continuously from 0% to 100% relative humidity.

Acknowledgements

PJ would like to thank Dr. James Wescott for his assistance with the computer programming. This work was financially supported by the EPSRC and National Power Innogy as part of their ongoing research into regenerative fuel cell technology.

References

1. H. L. YEAGER and A. STECK, *Journal of the Electrochemical Society* **128** (1981) 1880.
2. H. L. YEAGER, B. O'DELL and Z. TWARDOWSKI, *ibid.* **129** (1982) 85.
3. M. R. TANT, K. A. MAURITZ and G. L. WILKES, "Ionomers: Synthesis, Structure, Properties and Applications" (Chapman & Hall, London, 1997).
4. T. A. ZAWODZINSKI, T. E. SPRINGER, J. DAVEY, R. JESTEL, C. LOPEZ, J. VALERIO and S. GOTTESFELD, *Journal of the Electrochemical Society* **140**(7) (1993) 1981.
5. A. EISENBERG and H. L. YEAGER, "Perfluorinated Ionomer Membranes" (ACS Books, Washington, 1982).
6. T. D. GIERKE, G. E. MUNN and F. C. WILSON, *Journal of Polymer Science Part B-Polymer Physics* **19**(11) (1981) 1687.
7. E. J. ROCHE, M. PINERI, R. DUPLESSIX and A. M. LEVELUT, *ibid.* **19**(1) (1981) 1.
8. M. FUJIMURA, T. HASHIMOTO and H. KAWAI, *Macromolecules* **14**(5) (1981) 1309.
9. *Idem., ibid.* **15**(1) (1982) 136.
10. C. L. MARX, D. F. CAULFIELD and S. L. COOPER, *ibid.* **6** (1973) 344.
11. E. J. ROCHE, R. S. STEIN, T. P. RUSSELL and W. J. MACKNIGHT, *Journal of Polymer Science Part B-Polymer Physics*, **18** (1980) 1497.
12. W. J. MACKNIGHT, W. P. TAGGART and R. S. STEIN, *Journal of Polymer Science Symposium C* **45** (1974) 113.
13. J. KAO, R. S. STEIN, T. P. RUSSELL, W. J. MACKNIGHT and G. S. CARGILL, *Macromolecules* **7** (1974) 95.
14. S. RIEBERER and K. H. NORIAN, *Ultramicroscopy* **41** (1982) 225.
15. Z. PORAT, J. R. FRYER, M. HUXHAM and I. RUBINSTEIN, *Journal of Physical Chemistry* **99** (1995) 4667.
16. W. Y. HSU and T. D. GIERKE, *Journal of Membrane Science* **13**(3) (1983) 307.
17. H. S. SODAYE, P. K. PUJARI, A. GOSWAMI and S. B. MANOHAR, *Journal of Polymer Science Part B-Polymer Physics* **36**(6) (1998) 983.
18. *Idem., ibid.* **35**(5) (1997) 771.
19. G. DLUBEK, R. BUCHHOLD, C. HUBNER and A. NAKLADAL, *Macromolecules* **32**(7) (1999) 2348.
20. M. CHOMAKOVA-HAEFKE, R. NYFFENEGGER and E. SCHMIDT, *Applied Physics A* **59** (1994) 151.
21. A. LEHMANI, S. DURAND-VIDAL and P. TURQ, *Journal of Applied Polymer Science* **68**(3) (1998) 503.
22. G. H. McCAIN and M. J. COVITCH, *Journal of the Electrochemical Society* **131** (1984) 1350.
23. G. GEBEL, P. ALDEBERT and M. PINERI, *Polymer* **34** (1993) 333.
24. F. F. FAN and A. J. BARD, *Science* **270** (1995) 1849.
25. M. V. MIRKIN, *Analytical Chemistry News and Features A* **68** (1996) 177.
26. A. M. S. ELLIOTT, Unpublished research, 1999.

27. B. DREYFUS, G. GEBEL, P. ALDEBERT, M. PINERI, M. ESCOUBES and M. THOMAS, *Journal De Physique* **51**(12) (1990) 1341.
28. J. A. ELLIOTT, PhD thesis, University of Bristol, 1998.
29. J. A. ELLIOTT and S. HANNA, *Journal of Applied Crystallography* **32** (1999) 1069.
30. J. SKILLING and S. F.GULL, "Maximum Entropy and Bayesian Methods in Inverse Problems," edited by C. R. Smith and W. T. Grandy JR. (Dordrecht: Riedel, 1985) p. 83.
31. G. BINNIG, C. F. QUATE and C. GERBER, *Physics Review Letters* **56** (1986) 930.
32. T. J. MCMASTER, J. K. HOBBS, P. J. BARHAM and M. J. MILES, *Probe Microscopy* **1**(1) (1997) 43.
33. J. K. HOBBS, T. J. MCMASTER, M. J. MILES and P. J. BARHAM, *Polymer* **39**(12) (1998) 2437.
34. B. RATNER and V. V. TSUKRUK, "Scanning Probe Microscopy in Polymers" (ACS Books, Washington, 1998).
35. P. J. JAMES, T. J. MCMASTER, J. M. NEWTON and M. J. MILES, *Polymer* **41**(11) (2000) 4223.
36. K. L. BABCOCK and C. B. PRATER, D.I. Application Note A12, 1995.
37. J. TAMAYO and R. GARCIA, *Langmuir* **12** (1996) 4431.
38. P. LECLERE, R. LAZZARONI, J. L. BREDAS, J. M .YU, P. DUBOIS and R. JEROME, *ibid.* **12** (1996) 4317.
39. A. J. HOWARD, R. R. RYE and J. E. HOUSTON, *Journal of Applied Physics* **79** (1996) 1885.
40. M. H. WHANGBO, S. N. MAGONOV and H. BENGEL, *Probe Microscopy* **1** (1997) 23.
41. J. TAMAYO and R. GARCIA, *Applied Physics Letters* **71** (1997) 2394.
42. R. GARCIA, J. TAMAYO, M. CALLEJA and F. GARCIA, *Applied Physics A-Materials Science & Processing* **66**(PtISS) (1998) S309.
43. J. P. CLEVELAND, B. ANCZYKOWSKI, A. E. SCHMID and V. B. ELINGS, *Applied Physics Letters* **72**(20) (1998) 2613.
44. J. TAMAYO and R. GARCIA, *ibid.* **73**(20) (1998) 2926.
45. J. A. ELLIOTT, S. HANNA, A. M. S. ELLIOTT and G. E. COOLEY, *Macromolecules* **33** (2000) 4161.

Received 1 February
and accepted 26 February 2000

DIRECT POLYMERIZATION OF SULFONATED POLY(ARYLENE ETHER) RANDOM COPOLYMERS AND POLY(IMIDE) SULFONATED POLY (ARYLENE ETHER) SEGMENTED COPOLYMERS: NEW CANDIDATES FOR PROTON EXCHANGE MEMBRANE FUEL CELL MATERIAL SYSTEMS

Jeffrey B. Mecham

Dissertation submitted to the faculty of the Virginia Polytechnic Institute and State University in partial fulfillment of the requirements for the degree of

Doctor of Philosophy
in
Chemistry

James E. McGrath, Chair
Mark R. Anderson
John G. Dillard
Allan R. Shultz
James F. Wolfe

April 23, 2001
Blacksburg, Virginia

Keywords: Direct Copolymerization, Random Copolymer, Segmented Copolymer, Sulfonic Acid Sites, Poly(arylene ether), Poly(imide), Proton Exchange Membrane, Fuel Cell

DIRECT POLYMERIZATION OF SULFONATED POLY(ARYLENE ETHER) RANDOM COPOLYMERS AND POLY(IMIDE) SULFONATED POLY (ARYLENE ETHER) SEGMENTED COPOLYMERS: NEW CANDIDATES FOR PROTON EXCHANGE MEMBRANE FUEL CELL MATERIAL SYSTEMS

Jeffrey B. Mecham

Committee Chairman: Dr. James E. McGrath

Department of Chemistry

ABSTRACT

Commercially available 4,4'-dichlorodiphenylsulfone (DCDPS) was successfully disulfonated with fuming sulfuric acid to yield 3,3'-disodiumsulfonyl-4,4'-dichlorodiphenylsulfone (SDCDPS). Subsequently, DCDPS and SDCDPS were systematically reacted with 4,4'-biphenol under nucleophilic step polymerization conditions to generate a series of high molecular weight, film-forming, ductile, ion conducting copolymers. These were converted to the acid form and investigated as proton exchange membranes for fuel cells. Hydrophilicity increased with the level of sulfonation. However, water sorption increased gradually until about 50 mole percent SDCDPS was incorporated, and thereafter showed a large increase to yield water soluble materials for the 100% SDCDPS system. Atomic force microscopy (AFM) confirmed that the morphology of the copolymers displayed continuity of the hydrophilic phase at 60 mole percent SDCDPS. Conductivity measurements in the 40-50 mole percent SDCDPS range, where excellent mechanical strength was maintained, produced values of 0.1 S/cm or higher which were comparable to the control, Nafion™. These compositions also show a high degree of compatibility with heteropolyacids such as phosphotungstic acid. These inorganic compounds provide a promising mechanism for obtaining

conductivity at temperatures well above the boiling point of water and membrane compositions containing them are being actively pursued.

The water soluble 100% SDCDPS system was further investigated by successfully functionalizing the endgroups to afford aromatic amines via appropriate endcapping with *m*-aminophenol. Oligomers and polymers from 5-30 kg/mole number average molecular weight were synthesized and well characterized by NMR spectroscopy, endgroup titrations and size exclusion chromatography. The diamino-telechelic sulfonated segment was reacted with several dianhydrides and diamines to produce multiblock, hydrophobic polyimide-hydrophilic sulfonated polyarylene ether copolymers. Both ester-acid and amic acid synthesis routes were utilized in combination with spin-casting and bulk imidization. A series of tough, film-forming segmented copolymers was prepared and characterized. AFM measurements demonstrated the generation of quite well defined, nanophase-separated morphologies which were dependent upon composition as well as aging in a humid environment. Characterizations of the segmented copolymers for conductivity, and water and methanol sorption were performed and comparisons to state-of-the-art perfluorinated Nafion™ systems were made. It is concluded that the segmented or block systems have the potential to enhance certain desirable PEM characteristics in fuel cells, particularly those related to swelling, retention of mechanical strength at elevated temperatures, and critical adhesion issues in membrane electrode assemblies.

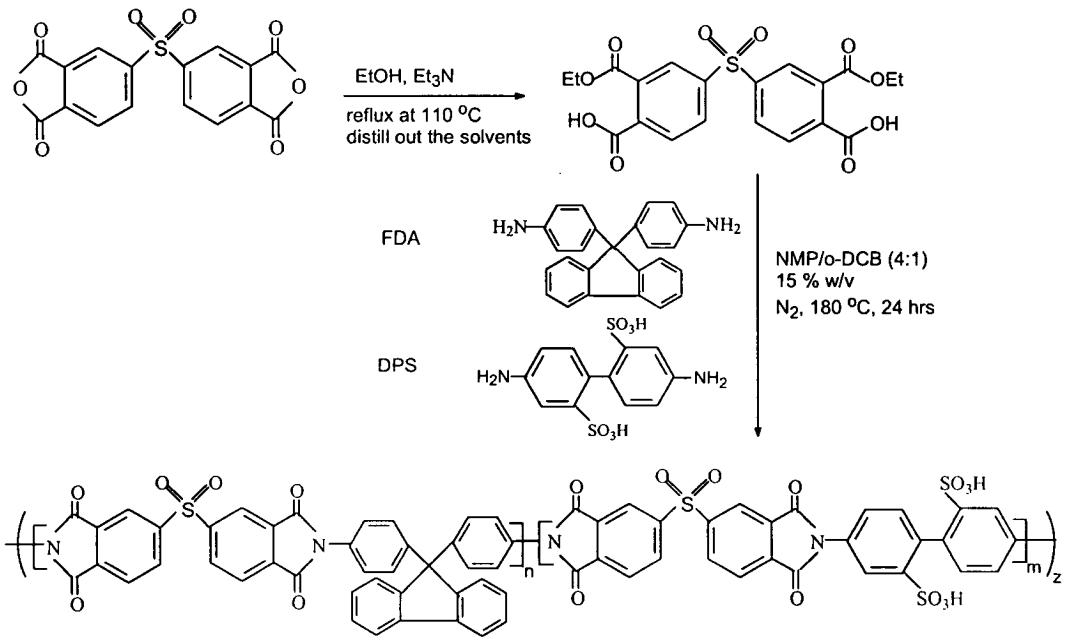

Figure 2.29: 5-membered Ring Polyimide containing Pendant Sulfonate Groups

films to remain stable during the chemical conversion from sulfonic sodium salt to sulfonic acid is crucial if the films are to be used as a PEM in a polymer electrolyte fuel cell. The triethyl ammonium salt form is needed to provide stability of the sulfonated monomers during polymerization, while the acid form is needed for proton conductivity when used as a PEM in a fuel cell. The polyimide containing 40 mole percent sulfonated diamine had an ion-exchange capacity very close to that of Nafion, while conductivity measurements yielded a value of 0.09 S/cm, which is near the value of Nafion at 0.1 S/cm.

b. Chemical Modification of Polymers

An alternate approach to introducing ionic functionalities into polymeric systems involves subsequent polymer modification reactions. This approach is especially suitable for the introduction of sulfonate groups via sulfonation of aromatic or unsaturated sites. The simplest example is the sulfonation of poly (styrene) by using either acetyl sulfate or sulfur trioxide/triethylsulfate, shown in figure 2.31.[102] Acetyl sulfate is the reaction product of acetic anhydride and sulfuric acid. In the case of poly (styrene), a pendant sulfonate is formed, but main chain aromatic rings can also be functionalized with the sulfonic acid moiety.[103]

The sulfonation of ethylene-propylene-diene (EPDM) monomer systems has generated considerable commercial interest.[104] By using Ziegler-Natta catalysis techniques, a random copolymerization of the three monomers can be achieved.[105] One of the preferred dienes is 5-ethylidene-2-norbornene which contains an endo- and exocyclic group. Polymerization proceeds through the endocyclic double bond and the exocyclic unsaturated site is available for subsequent sulfonation, as shown in figure

---

[102] Makowski, H. S.; Lundberg, R. D.; Westerman, L.; Bock, J. In *Ions in Polymers*; Eisenberg, A., Ed.; Am. Chem. Soc.: Wash., D.C., 1980; Vol. 187.

Makowski, H. S.; Lundberg, R. D.; Singhal, G.; Exxon; U.S. 3,870,841; 1975

[103] Johnson, B. C.; Yilgor, I.; Tran, C.; Iqbal, M.; Wightman, J.; Lloyd, D.; McGrath, J. E. *J. Polym. Sci. Polym. Chem. Ed.* 1984, *22*.

[104] Makowski, H. S.; Lundberg, R. D.; Westerman, L.; Bock, J. *Polymer Preprints* 1978, *19*, 292.

[105] McGrath, J. E. In *Encyclopedia of Chemical Technology*; 3rd ed.; Wiley Interscience, 1979; Vol. 8.

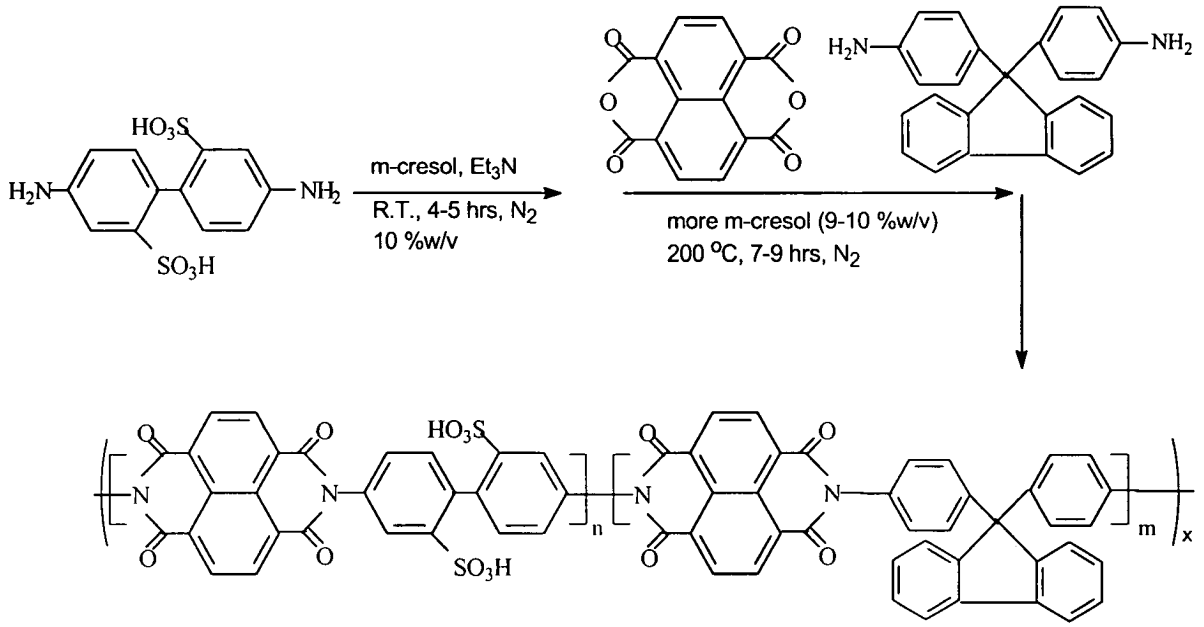

Figure 2.30: 6-membered Ring Polyimide containing Pendant Sulfonate Groups

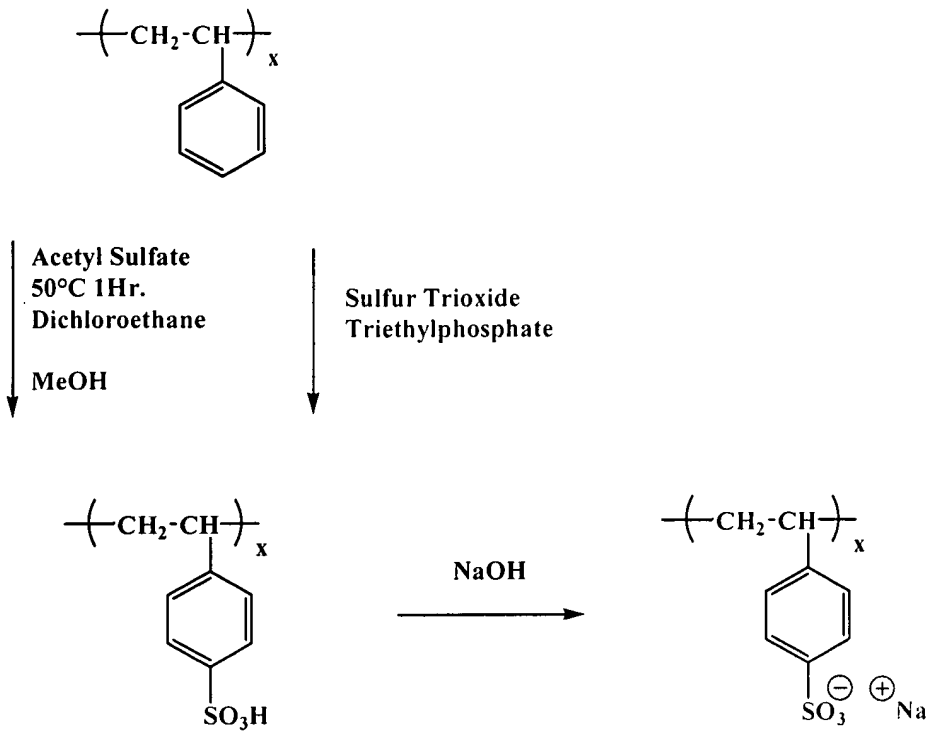

Figure 2.31: Sulfonation of Poly (styrene)

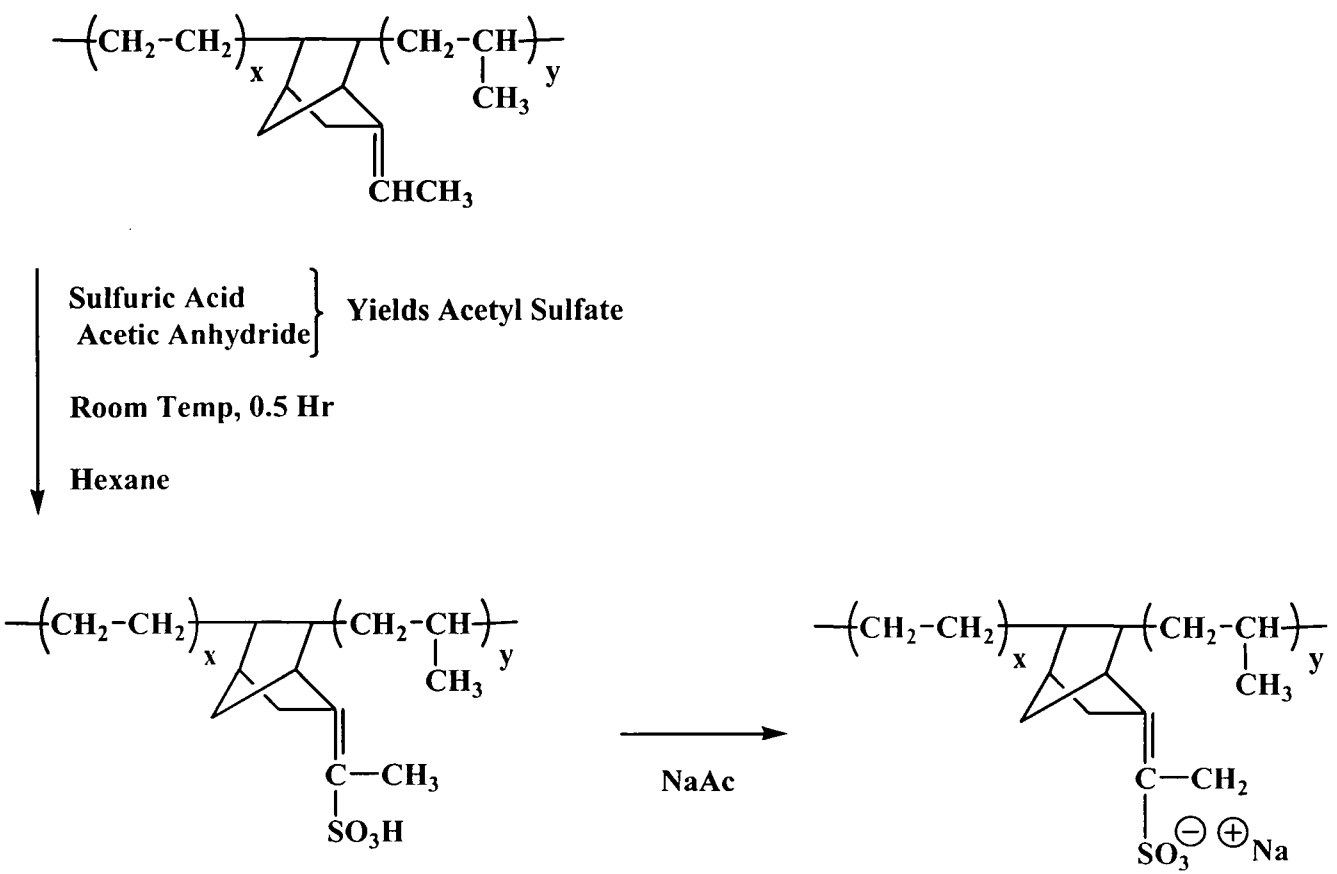

Figure 2.32: Sulfonation of EPDM[103]

General Motors, Volkswagen, Nissan, Honda and Volvo among the largest participants in research and development. It has been projected that the number of vehicles (worldwide) will increase from the current level of 600 million to 1 billion by 2015.[116] The American Methanol Institute recently estimated that by the year 2010, automakers will have introduced at least 2 million methanol fuel cell vehicles worldwide, with the number surpassing 35 million by 2020. Fuel cell vehicle introduction will focus initially on the three states in the U.S. requiring the sale of zero emission vehicles by 2003 (California, New York and Massachusetts) as well as Germany and Japan. These are areas of high population that are candidates for early acceptance of alternative fuel vehicles because they tend to have higher levels of pollution and offer maximum scale efficiencies for the first wave of methanol fuel infrastructure.

The vast quantity of natural gas in the world ensures the availability of feedstock to produce the methanol needed for the future fleet of DMFC vehicles. In 1996, reserves stood at 49,912 trillion cubic feet (TCF) with annual consumption of 78 TCF. With a fleet of 35 million vehicles consuming 15.4 billion gallons of methanol annually (at 441 gal/yr each), this would create a demand for 1.4 TCF of natural gas per annum, which is only 2 % of current annual consumption.[176] It can be argued that the methanol supply and delivery infrastructure can be adjusted to meet future DMFC vehicle demands.

7. Water Uptake and Protonic Conductivity in Sulfonated Polymer Membranes

a. Water Uptake of Nafion Fluoropolymer

Proton transport in ionic polymer membranes, especially when in the acid form, is largely influenced by the water content of the membrane. Ionic membranes behave like insulators in the dry state, but become conductive as a function of the water content when hydrated. Various studies have been conducted as to the minimum water content threshold for measurable conductivity. Several researchers have shown that a minimum of 6 or 7 water molecules are needed per sulfonic acid site to generate sufficient

[116] Lewis, R.; Dolan, G. In *Fuel Cell Power for Transportation*; Seaba, J., Stobart, R., Eds.; Society of Automotive Engineers: Warrendale, PA, 1999; Vol. 1425, p 22.

conductivity for use as a PEM.[117] Among the ionic polymers with high protonic conductivity, the activation energy of proton conduction of Nafion perfluoropolymer is low in comparison to other polymers[118] which may be due to the state of the water in the membrane. In a fuel cell using proton exchange membranes, the water content is controlled by humidification of the gas streams at each side of the membrane. Under these conditions, it has been shown[119] that the proton conductivity reaches a maximum at temperatures between 55-70°C while water contents approach a minimum. This work established that at lower temperatures between 25-50°C, a variation in water content is less important than a temperature increase, which plays an important role in the kinetics of proton motion in the polymer membrane.

Work by Zawodzinski *et. al.* also involved investigation of water uptake of Nafion 117 membranes.[120] Water uptake was studied by investigating membranes that were initially fully hydrated and were then exposed to a variety of drying conditions: 1) dried at room temperature under vacuum; 2) condition 1 followed by vacuum drying at 105°C for an hour; 3) drying at room temperature over P_2O_5; and 4) condition 3 followed by vacuum drying at 105°C. Earlier work by Bunce *et al.*[121] has shown that the water content after drying under condition 1 resulted in $\lambda = 1$ (where λ = number of moles of water per mole of sulfonic acid group in polymer), whereas drying conditions 2, 3 and 4 resulted in total dehydration. The extent of rehydration of the membranes was dependent on the drying condition. Figure 2.40 illustrates the water uptake as a function of time and compares a film that was dried at room temperature under vacuum versus a film dried under vacuum at 105°C. The membrane that was dried at room temperature contained the

---

[117] Yeo, R. S. *J. Electrochem. Soc.* **1983**, *130*, 533.
Pourcelly, G.; Oikonomou, A.; Hurwitz, H. D.; Gavach, C. *J. Electroanal. Soc.* **1990**, *287*, 43.
Randin, J. *J. Electrochem. Soc.* **1982**, *129*, 1215.

[118] Yeo, R. S. *J. Electrochem. Soc.* **1983**, *130*, 533.

[119] Reike, P. C.; Vanderborgh, N. E. *J. Membrane Sci.* **1987**, *32*, 313.

[120] Zawodzinski, T.; Derouin, C.; Radzinski, S.; Sherman, R. J.; Smith, V. T.; Springer, T. E.; Gottesfeld, S. *J. Electrochem. Soc.* **1993**, *140*, 1041.

[121] Bunce, N.; Sondheimer, S.; Fyfe, C. A. *Macromolecules* **1986**, *19*, 333.

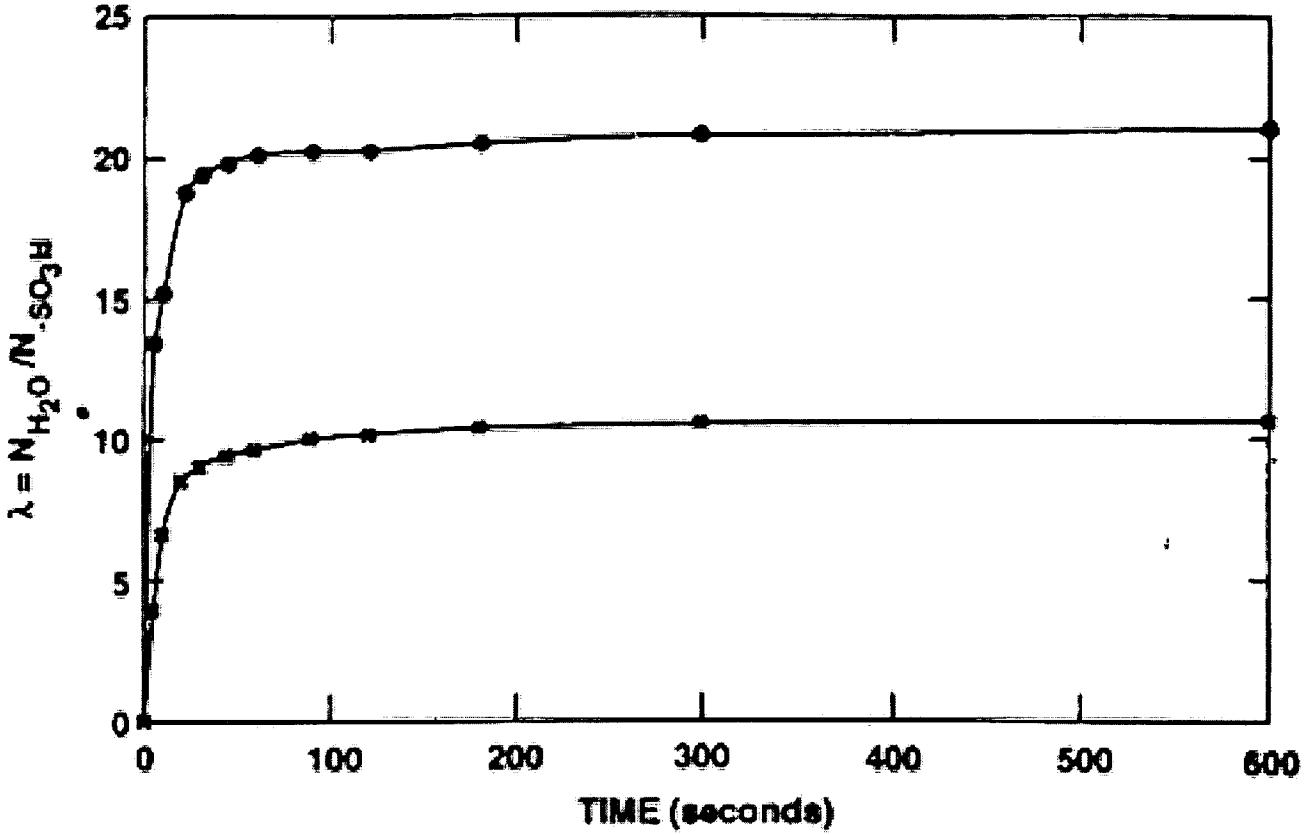

Figure 2.40: Water uptake as a function of time after drying at room (•)and elevated temperature[122]

[122]) Zawodzinski, T.; Derouin, C.; Radzinski, S.; Sherman, R. J.; Smith, V. T.; Springer, T. E.; Gottesfeld, S. *J. Electrochem. Soc.* **1993**, *140*, 1041.

Table 2.2: Water uptake of Nafion 117 using various methods[123]

Water temperature[e] (°C)	Water uptake (H_2O/equivalent) Drying method			
	1[a]	2[b]	3[c]	4[d]
27	21.3	11.3	21.0	12
65	21.0	15.2	—	—
80	20.7	15.9	—	—

[a] Dried under vacuum at room temperature.
[b] Dried under vacuum at room temperature followed by 1 h at 105°C.
[c] Dried over P_2O_5 at room temperature.
[d] Dried over P_2O_5 at room temperature followed by 1 h at 105°C.
[e] Temperature of membrane rehydration.

[123] Zawodzinski, T.; Derouin, C.; Radzinski, S.; Sherman, R. J.; Smith, V. T.; Springer, T. E.; Gottesfeld, S. *J. Electrochem. Soc.* **1993**, *140*, 1041.

same amount of water after rehydration as it did prior to drying ($\lambda = 22$), whereas the water uptake of the Nafion membrane dried at elevated temperature was only half of the initial value. Interestingly, the water uptake of the membrane dried at room temperature was independent of the water temperature, while the water content of the membrane dried at elevated temperature was a function of the water temperature. The results are summarized in table 2.2.

The most likely explanation for the above results involves the formation and dissociation of the ionic clusters as the membrane is dried. The pretreatment of the Nafion 117 membranes were boiled in 0.5M sulfuric acid for an hour, followed by an hour in boiling deionized water to remove any excess acid. The pretreatment should provide enough thermal energy to form hydrated ionic clusters, but reorientation of the polymer during the drying step is required for the clusters to be broken up, which requires enough energy for Nafion ionic side chains motion. As long as water is present, the sulfonic acid moiety remains ionized, but as the membrane becomes dehydrated, the ionic clusters shrink in size and remain aggregated. As the final traces of water are removed, the sulfonic acid group is no longer ionized, the coulombic barrier to reorientation is no longer present, and the clusters can be dissociated at temperatures near the glass transition of the polymer. This explanation applies the same principles suggested by Eisenberg, where cluster formation is a balance between the ionic dipole interactions that favor formation and elastic forces that disrupt their formation.[124]

The dependence of membrane rehydration on drying conditions has important implications if they are used as an MEA in a fuel cell. One method of MEA fabrication requires hot-pressing a pair of gas diffusion electrodes that containing a Nafion dispersion onto the surface of the Nafion 117 membrane at 120°C. This process causes complete dehydration of the membrane causing a potential decrease in λ. This may have a negative effect on the maximum attainable conductivity of the membrane, since conductivity and water uptake have a roughly linear relationship.

---

[124] Eisenberg, A. *Macromolecules* **1970**, *3*, 147.

b. Protonic Conductivity of Nafion Fluoropolymer

Although many properties of Nafion fluoropolymer have been investigated[125], proton conductivity details are reported less frequently. Some of the pivotal work has been performed by Zawodzinski *et. al.* [126]and Kreuer *et. al.*[127]

The conductivity of Nafion 117[128] has been reported by Zawodzinski *et. al.* as a function of water content (figure 2.41) and temperature (figure 2.42). At 30°C, the conductivity decreases in a generally linear fashion with decreasing water content. The value of the conductivity, 0.06 S/cm, where $\lambda = 14$ (where λ = number of moles of water per mole of sulfonic acid group in polymer), agrees with data reported by Rieke *et. al.*[129] An Arrhenius plot illustrating the temperature dependence over the range of 25-90°C is shown in figure 2.42. The observation that the plot is not linear illustrates the possibility that various mechanisms may be involved in protonic motion through the polymer membrane which can be calculated from the conductivity data. The diffusion coefficient of H^+ can be calculated from the conductivity by using the Nernst-Einstein Equation[130], below. This equation was derived by W. Nernst in 1888[131] and was originally used to calculate the diffusion coefficient of ions in dilute solutions.

---

[125] Pourcelly, G.; Gavach, C. In *Proton Conductors*; Colomban, P., Ed.; Cambridge University Press: London, 1992; p 295.
Eisenberg, A.; Yeager, H. L. *Perfluorinated Ionomer Membranes*; ACS Symposium Series #180:, 1982.

[126] Zawodzinski, T.; Derouin, C.; Radzinski, S.; Sherman, R. J.; Smith, V. T.; Springer, T. E.; Gottesfeld, S. *J. Electrochem. Soc.* **1993**, *140*, 1041.
Zawodzinski, T.; Neeman, M.; Sillerud, L. O.; Gottesfeld, S. *J. Phys. Chem.* **1991**, *95*, 6040.

[127] Kreuer, K. D.; Dippel, T.; Meyer, W.; Maier, J. In *Mat. Res. Soc. Symp. Proc.*, 1993; Vol. 293, p 273.

[128] Zawodzinski, T.; Derouin, C.; Radzinski, S.; Sherman, R. J.; Smith, V. T.; Springer, T. E.; Gottesfeld, S. *J. Electrochem. Soc.* **1993**, *140*, 1041.

[129] Reike, P. C.; Vanderborgh, N. E. *J. Membrane Sci.* **1987**, *32*, 313.

[130] Perry, R. H.; Chilton, C. H. *Chemical Engineer's Handbook*; 5th ed.; McGraw-Hill: New York, 1973.

[131] Nernst, W. *Z. Phys. Chem* **1888**, *2*, 613.

$$D_0 = RT(l^+ * l^- / \Lambda_0)(z^+ + z^-)(z^+ * z^-)$$

Where:

D_0	Diffusivity of molecule at infinite dilution (ionic pair), in cm^2/sec
R	Gas constant, $8.931 * 10^{-10}$
T	Temperature, in Kelvin
l^+	Cationic conductance at infinite dilution, in S/equivalent
l^-	Anionic conductance at infinite dilution, in S/equivalent
Λ_0	Electrolyte conductance in infinite dilution, in S/equivalent
z^+	Valence of cation (absolute, no sign)
z^-	Valence of anion (absolute, no sign)

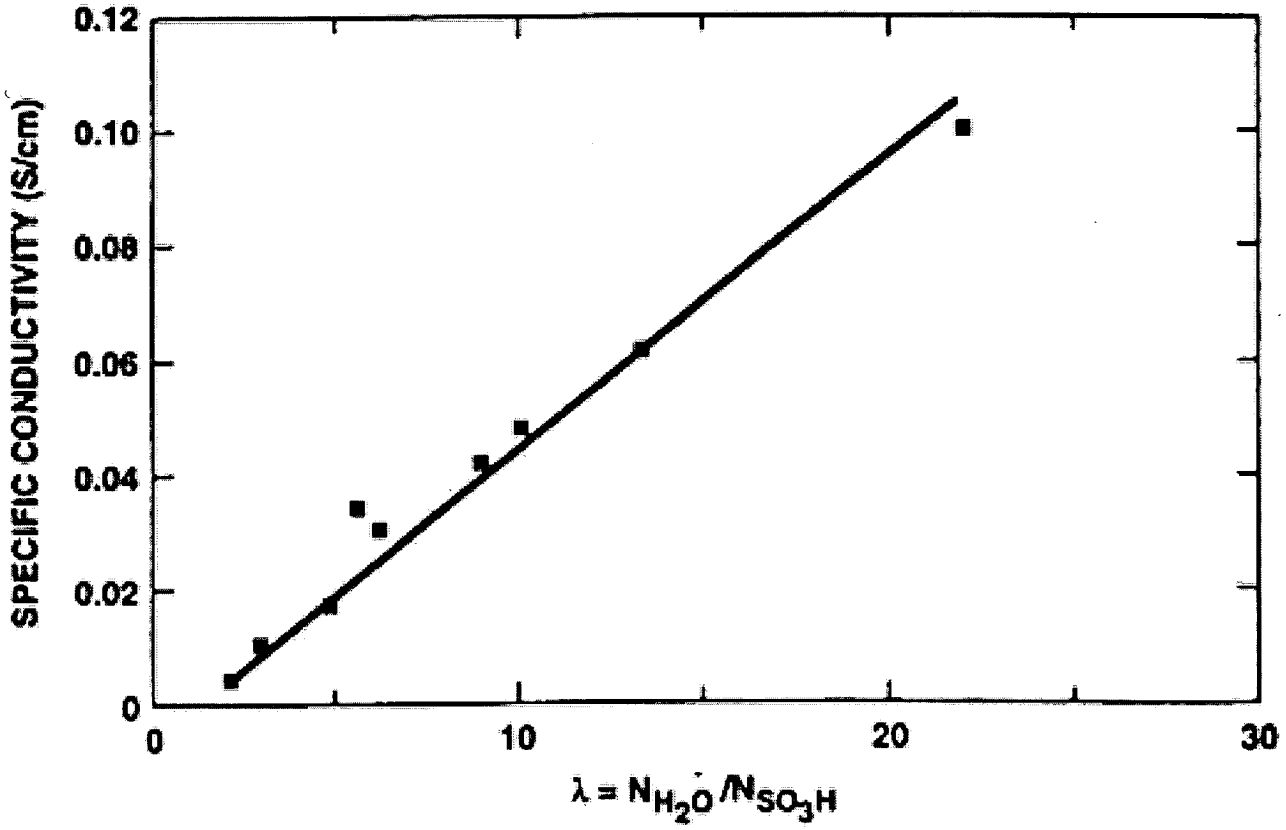

Figure 2.41: Nafion 117 Membrane Conductivity as a function of Water Content[181]

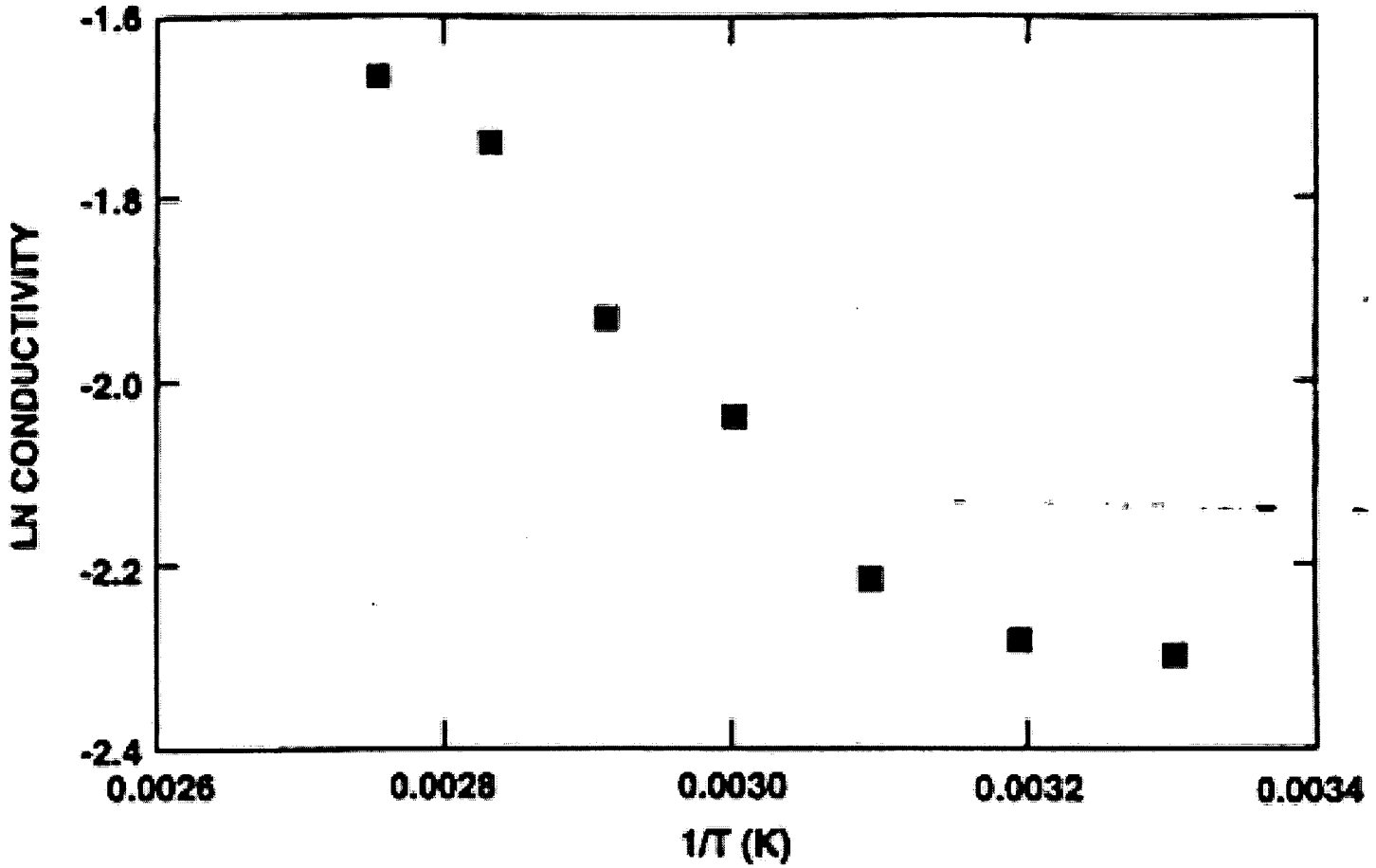

Figure 2.42: Arrhenius plot illustrating the temperature dependence of protonic conductivity in Nafion 117 between 25-90°C[181]

MENU
Home
Term of the Day
New Terms
New Links
Quick Reference
Did You Know?
Search Tool
Tech Support
Webopedia Jobs
About Us
Link to Us
Advertising

Compare Prices: go
HardwareCentral

Talk To Us
Submit a URL
Suggest a Term
Report an Error

internet.com
Developer
Downloads
International
Internet Lists
Internet News
Internet Resources
IT
Linux/Open Source
Small Business
Windows Technology
Wireless Internet
xSP Resources

Search internet.com
Advertise
Corporate Info
Newsletters
Tech Jobs
E-mail Offers

internet commerce
Be a Commerce Partner

phase change disk

Last modified: Saturday, July 05, 1997

A type of rewritable optical disk that employs the phase change recording method. Using this technique, the disk drive writes data with a laser that changes spots on the disk between amorphous and crystalline states. An optical head reads data by detecting the difference in reflected light from amorphous and crystalline spots. A medium-intensity pulse can then restore the original crystalline structure.

Magneto-optical and dye-polymer technologies offer similar capabilities for developing re-writable optical disks.

•E-mail this definition to a colleague•

*For internet.com pages about **phase change disk** CLICK HERE. Also check out the following links!*

LINKS = Great Page!

Related Categories

Disk Drives

Related Terms

class

magneto-optical (MO) drive

optical disk

solid ink-jet printer

worm

(Webopedia)
Give Us Your Feedback

Theories for the dielectric constant.

G. van der Zwan

December 4, 2003

1 Maxwell equations and constitutive relations.

The Maxwell equations in a polarizable, magnetizable medium, in which also charges are present, can be written in the following form:

$$\begin{aligned} \vec{\nabla}\cdot\vec{B} &= 0 \\ \vec{\nabla}\cdot\vec{E} &= \frac{1}{\epsilon_0}\left(\rho-\vec{\nabla}\cdot\vec{P}\right) \\ \vec{\nabla}\times\vec{E}+\frac{\partial\vec{B}}{\partial t} &= 0 \\ \vec{\nabla}\times\vec{B}-\frac{1}{c^2}\frac{\partial\vec{E}}{\partial t} &= \mu_0\left(\vec{j}+\vec{\nabla}\times\vec{M}-\frac{\partial\vec{P}}{\partial t}\right) \end{aligned} \tag{1.1}$$

We neglect magnetization effects, thus setting $\vec{M}=0$. The following relation is always true:

$$\vec{D}=\epsilon_0\vec{E}+\vec{P} \tag{1.2}$$

Therefore the equations can also be written as

$$\begin{aligned} \vec{\nabla}\cdot\vec{B} &= 0 \\ \vec{\nabla}\cdot\vec{D} &= \rho \\ \vec{\nabla}\times\vec{E}+\frac{\partial\vec{B}}{\partial t} &= 0 \\ \vec{\nabla}\times\vec{H}-\frac{\partial\vec{D}}{\partial t} &= \vec{j} \end{aligned} \tag{1.3}$$

where $\vec{B}=\mu_0\vec{H}$ in case the magnetization is zero.
The charge conservation equation follows from taking the divergence of the last equation, using that $\vec{\nabla}\cdot(\vec{\nabla}\times\vec{H})=0$, and inserting the second equation. We thus get

$$\frac{\partial\rho}{\partial t}=-\vec{\nabla}\cdot\vec{j} \tag{1.4}$$

In the remainder of this section we use Fourier transform language, meaning that all partial derivatives with respect to time are replaced by $-i\omega$.

We now assume the following two constitutive, linear relations:

$$\vec{j}(\vec{r},\omega) = \kappa(\omega)\vec{E}(\vec{r},\omega) \tag{1.5}$$

and

$$\vec{D}(\vec{r},\omega) = \epsilon_0\epsilon(\omega)\vec{E}(\vec{r},\omega) \tag{1.6}$$

Eliminating density ρ, current $\vec{j}$, and $\vec{D}$ in virtue of $\vec{E}$, we can write these equations as

$$\vec{\nabla} \times \vec{E}(\vec{r},\omega) - i\omega\mu_0\vec{H}(\vec{r},\omega) = 0 \tag{1.7}$$

and

$$\vec{\nabla} \times \vec{H}(\vec{r},\omega) + i\omega\left(\epsilon_0\epsilon(\omega) - \frac{\kappa(\omega)}{i\omega}\right)\vec{E}(\vec{r},\omega) = 0 \tag{1.8}$$

whereas for the charge density we find that

$$\rho(\vec{r},\omega) = \frac{\kappa(\omega)}{i\omega}\vec{\nabla}\cdot\vec{E}(\vec{r},\omega) \tag{1.9}$$

Taking once more the curl of eq. (1.8), using that

$$\vec{\nabla} \times (\vec{\nabla} \times \vec{H}) = \vec{\nabla}(\vec{\nabla}\cdot\vec{H}) - \Delta\vec{H} = -\Delta\vec{H} \tag{1.10}$$

in view of the first of eqs. (1.3) and the absence of magnetization, we find:

$$-\Delta\vec{H}(\vec{r},\omega) + i\omega\left(\epsilon_0\epsilon(\omega) - \frac{\kappa(\omega)}{i\omega}\right)\vec{\nabla} \times \vec{E}(\vec{r},\omega) = 0 \tag{1.11}$$

Subsequent substitution of (1.7) the yields:

$$\Delta\vec{H}(\vec{r},\omega) + \frac{\omega^2}{c^2}\left(\epsilon(\omega) - \frac{\kappa(\omega)}{i\omega\epsilon_0}\right)\vec{H}(\vec{r},\omega) = 0 \tag{1.12}$$

This is a wave equation for the vector field $\vec{H}$, with dispersion relation:

$$k^2 = \frac{\omega^2}{c^2}\left(\epsilon(\omega) - \frac{\kappa(\omega)}{i\omega\epsilon_0}\right) \tag{1.13}$$

We can derive a similar equation for the electric field: take the curl of eq. (1.7) and use the equivalent of relation (1.10), we get:

$$\Delta\vec{E}(\vec{r},\omega) + \frac{\omega^2}{c^2}\left(\epsilon(\omega) - \frac{\kappa(\omega)}{i\omega\epsilon_0}\right)\vec{E}(\vec{r},\omega) = \frac{i\omega}{\kappa(\omega)}\vec{\nabla}\rho(\vec{r},\omega) \tag{1.14}$$

where we also used eqs. (1.8) and (1.9).
This is again a wave equation, now for the electric field with the same dispersion relation as above, but with a source term.
The assumption is now that the charges move slow compared to changes in the electro–magnetic field. In that case we can neglect the source term. Alternatively we can state that the transverse waves are unaffected by the charge distribution, the longitudinal wave probably decay faster as a function opf the distance to the sample. A bigger problem is the frequency dependence of κ. Assuming that it can be replace by its zero–frequency value means that the charges can follow the electric field. For microwave frequencies that is $10^{10} - 10^{12}s^{-1}$ this seems strange.

2 The dielectric constant of a gas of non–polarizable molecules.

The simplest theory for the dielectric constant is that for a gas consisting of non–polarizable dipoles.
The dielectric constant can be related to the ratio of the polarization, or macroscopic dipole moment per unit volume of a system, and the electric field $\vec{E}$ in the following way:

$$\vec{P}(\vec{r}) = \epsilon_0 \chi \vec{E}(\vec{r}) = \epsilon_0(\epsilon - 1)\vec{E}(\vec{r}) \tag{2.1}$$

Note that $\vec{P}$ is dipole moment per volume, which makes χ a dimensionless quantity.
In reality χ gives the relation between electric field and polarization, where the electric field $\vec{E}$ is not necessarily equal to the external field $\vec{E}_e$, but is modified by the presence of a polarizable medium.
We therefore have to calculate the polarization for a given external field to obtain ϵ, as well as the internal electric field.
For a low density gas of polar, non–polarizable molecules the interaction between the molecules can be neglected, and we only need the response of one dipole to an electric field.
For the moment we assume that the internal field is equal to the external field. Since we are in an equilibrium situation, the probability of finding a dipole $\vec{\mu}$ with given orientation in a field $\vec{E}_e$ is determined by the Boltzmann factor:

$$P(\cos\vartheta) = \frac{e^{\beta\mu E_e \cos\vartheta}}{\int_{-1}^{1} \cos\vartheta e^{\beta\mu E_e \cos\vartheta}} \tag{2.2}$$

where ϑ is the angle between dipole and field. The average dipole moment is then determined by

$$\langle\cos\vartheta\rangle = \int_{-1}^{1} \cos\vartheta \cos\vartheta P(\cos\vartheta) = \frac{\mu E_e}{3k_B T} \tag{2.3}$$

where we used the small field approximation, that is, expanded the exponential to lowest relevant order.
This means that we can write the average dipole moment as:

$$\langle\vec{\mu}\rangle = \frac{\mu^2}{3k_B T}\vec{E}_e \tag{2.4}$$

Consequently the polarization of the gas is given by:

$$\vec{P} = \frac{N}{V}\vec{\mu} = \rho\frac{\mu^2}{3k_B T}\vec{E}_e \tag{2.5}$$

where ρ is here the density of the gas. Therefore the dielectric constant is given by:

$$\epsilon - 1 = \frac{N\mu^2}{3\epsilon_0 k_B T} \tag{2.6}$$

again assuming that internal and external field are equal.

One wonders whether this can be taken a step further. After all the polarization causes an electric field, so that the field actually felt by the dipoles is different. If there is a polarization $\vec{P}$, every volume element $dV = d\vec{r}$ has a dipole moment $\vec{P}d\vec{r}$. A dipole at position $\vec{r}$ causes an electric field at position $\vec{r}'$ given by:

$$\frac{1}{4\pi\epsilon_0 R^3}\left(\mathbf{1} - 3\frac{\vec{R}\vec{R}}{R^2}\right)\cdot\vec{P}(\vec{r})d\vec{r} \tag{2.7}$$

where

$$\vec{R} = \vec{r} - \vec{r}' \tag{2.8}$$

Since the system is infinite, we can calculate the field at the origin, and since the polarization is constant, the integral can easily be calculated: the field due to polarization is equal to

$$\vec{E}_P = \frac{1}{4\pi\epsilon_0}\vec{P}\cdot\int d\vec{\Omega}\left(\mathbf{1} - 3\vec{\Omega}\vec{\Omega}\right)\int dr\,\frac{1}{r} \tag{2.9}$$

This does not work very well, unless we exclude a sphere or something around the origin to avoid infinities. The reason is that in this method we allow polarization at the position we measure the field. Anther possibility would be to take individual dipoles, connected to the molecules, and perform an average over the positions of the molecules. This also leads to infinities, since there is always a finite probability of finding the molecule at the origin. In addition we have a problem for large values of r, which is a consequence of the long range character of the electrical forces. No easy way to get around that either unless we want to take the shape of the vessel in which this is all taking place into account. SO: problems all around with this approach. See in this context also the remark by Fixman [1], p. 2076.
Let's try the probability method though, and see what happens. Before that the following: Fröhlich [2] assumes in the derivation of the gas phase dielectric constant that the dipoles do not interact, on the bases of the assumption that if they are far enough apart, the interaction energy is small compared to k_BT. This means that

$$\frac{\mu^2}{4\pi\epsilon_0 r^3} << k_BT \tag{2.10}$$

where r is the distance between the dipoles. At room temperature $\sim 298\,K$, we have $k_BT \approx 4.11\times10^{-23}\,J$. For a $1\,D = 3.336\times10^{-30}\,Cm$ dipole we get $\mu^2/4\pi\epsilon_0 r^3 \approx 10^{-49}/r^3\,Jm^3$. This means that for the above condition to hold we must have:

$$r \gg 1.4\times10^{-9}\,m = 1.4\text{nm} \tag{2.11}$$

In fact we want the electric field due to the dipoles at the position of the central dipole also to be small compared to the external electric field.
The microscopic dipole density is given by:

$$\vec{p}(\vec{r}) = \sum_{i=1}^{N}\vec{\mu}_i\delta(\vec{r} - \vec{r}_i) \tag{2.12}$$

where $\vec{\mu}_i$ is the dipole moment of particle i and $\vec{r}_i$ its position.

What we are interested in is the electric field at the position of a dipole due to all the other dipoles. The electric field at position $\vec{r}$ due to a dipole at position $\vec{r}_i$ is given by:

$$\vec{E}_i(\vec{r}) = \frac{1}{4\pi\epsilon_0|\vec{r}-\vec{r}_i|^3}\left(\mathbf{1} - 3\frac{(\vec{r}-\vec{r}_i)(\vec{r}-\vec{r}_i)}{|\vec{r}-\vec{r}_i|^2}\right)\cdot\vec{\mu}_i \tag{2.13}$$

Thus the total field at the position of dipole i is given by:

$$\vec{E}_p(\vec{r}_i) = \frac{1}{4\pi\epsilon_0}\sum_{j\neq i}\frac{1}{|\vec{r}_i-\vec{r}_j|^3}\left(\mathbf{1} - 3\frac{(\vec{r}_i-\vec{r}_j)(\vec{r}_i-\vec{r}_j)}{|\vec{r}_i-\vec{r}_j|^2}\right)\cdot\vec{\mu}_j \tag{2.14}$$

The next step is to perform averages: both over all positions of the dipoles, and over their orientation. Since we neglected interactions between the dipoles, they are uniformely distributed around the central dipole.
Using result (2.4), but now with the orienting field equal to the sum of field due to the polarization and external field, we get

$$\vec{E}_P = \frac{1}{4\pi\epsilon_0}\left\langle\sum_{j\neq i}\frac{1}{|\vec{r}_i-\vec{r}_j|^3}\left(1 - 3\frac{(\vec{r}_i-\vec{r}_j)(\vec{r}_i-\vec{r}_j)}{|\vec{r}_i-\vec{r}_j|^2}\right)\right\rangle\cdot\frac{\mu^2}{3k_BT}\left(\vec{E}_e+\vec{E}_P\right) \tag{2.15}$$

where we also used that the magnitude of all dipoles is equal. The remaining average is over the positions of the dipoles. This average is therefore defined as:

$$\langle\cdots\rangle = \int d\vec{r}^{N-1}P(\{\vec{r}^{N-1}\})(\cdots) \tag{2.16}$$

where $P(\{\vec{r}^{N-1}\})$ is the probability of finding a configuration $\{\vec{r}^{N-1}\}$. Note that strictly speaking we need the conditional probability of finding a configuration of $N-1$ particles, given a dipole at position $\vec{r}_1$, but since we neglected interactions between the molecules these are all independent, and in fact the probability of finding a particle anywhere is just $1/V$, where V is the volume of the system. Thus we can write the average as:

$$\left\langle\sum_{j\neq i}\frac{1}{|\vec{r}_i-\vec{r}_j|^3}\left(1 - 3\frac{(\vec{r}_i-\vec{r}_j)(\vec{r}_i-\vec{r}_j)}{|\vec{r}_i-\vec{r}_j|^2}\right)\right\rangle = \frac{N-1}{V}\int d\vec{r}\frac{1}{r^3}\left(1-3\frac{\vec{r}\vec{r}}{r^2}\right) \tag{2.17}$$

To get this result we used that all particles are equivalent, and therefore each of the terms, of which there are $N-1$, in the sum is the same, and furthermore that all positions are equivalent so that we can place the central particle to the origin.
In fact looking again at the earlier result, and this result, we notice that the angular integration equals zero. This can be understood in the following way: the probaility of finding a dipole with given orientation at position $\vec{r}_1$ is equal to finding a dipole with the same orientation at position $-\vec{r}_1$, since the orientation is assumed to be uncorrelated with the orientation of the central dipole. The field due to these dipoles is equal, but opposite, and therefore the total contribution to the field is zero. The whole exercise therefore showed taht we can indeed take the external field here as long as we neglect correlations between the dipoles.
But now I have a problem. This calculation of the inside field shows that there is no contribution due to the polarization when the field is constant. But it is always stated that

the electric field in a dielectric is reduced by the dielectric constant, so we also have the following for the field between two charged plates with charge density σ. The external, or vacuum field, is given by

$$\vec{E}_v = \frac{2\sigma}{\epsilon_0} \tag{2.18}$$

whereas the field in the dielectric is

$$\vec{E} = \frac{2\sigma}{\epsilon_0 \epsilon} \tag{2.19}$$

This means that the polarization must give rise to the difference between the two fields:

$$\vec{E}_P = \vec{E} - \vec{E}_v = \frac{2\sigma}{\epsilon_0} \frac{1-\epsilon}{\epsilon} \tag{2.20}$$

So according to this the electric field does change due to the presence of dipoles. If it is a correlation effect, than why are we allowed to neglect it in the derivation?
Another remaining problem, also present in the last derivation, is that, if the angular integration does not make the whole polarization effect vanish, we are still stuck with an infinite contribution due to the long range nature of the electrical forces.

3 The dielectric constant of a gas of polarizable molecules.

The first refinement can be made by making the molecules polarizable. This means that the dipole itself responds to the field by becoming larger. This enlargement is measured by the polarizability α. In that case the average dipole moment in an external field is given by

$$\langle \vec{\mu} \rangle = \frac{\mu^2}{3k_B T} \vec{E} + \alpha \vec{E} = \left(\alpha + \frac{\mu^2}{3k_B T} \right) \vec{E} \tag{3.1}$$

Thus we get for the static dielectric constant:

$$\epsilon - 1 = \frac{\rho \mu^2}{3\epsilon_0 k_B T} + \frac{\rho \alpha}{\epsilon_0} \tag{3.2}$$

Introducing the high frequency dielectric constant ϵ_∞ as

$$\epsilon_\infty - 1 = \frac{\rho \alpha}{\epsilon_0} \tag{3.3}$$

we can write the previous expression in the form:

$$\epsilon - \epsilon_\infty = \frac{\rho \mu^2}{3\epsilon_0 k_B T} \tag{3.4}$$

4 A dilute solution of dipoles in a polarizable medium.

The next step is to consider a dilute solution of dipoles in a polarizable medium. The dipoles are so far apart that they still do not have direct interaction, but since the medium is polarizable, we have to account for the fact that the internal field is different from the external field, and in addition that the reaction field of the dipoles influences the dipole moment if they are themselves polarizable.

5 Dielectric constant according to Debye.

Debye [3] starts out to find an explanation for the temperature dependence of the dielectric constant. Up to that time it was apparently customary to think of the dielectric behavior as resulting from the displacement of charges within an isolator, and then the dielectric constant does not depend on temperature. Rather than abolishing statistical mechanics Debye prefers to assume that in an isolator we do not just have bound charges but also permament dipole moments, and with that hypothesis he can explain the temperature dependence, on the basis of classical statistical mechanics.
On the basis of that hypothesis he basically derives eq. (3.2) with one important difference: for the field actually felt by the molecule, the directing field he does not use the external field, but a field derived by Lorentz (the so–called Lorentz field) which is given by:

$$\vec{E} = \vec{E}_e + \frac{1}{3\epsilon_0}\vec{P} = \frac{\epsilon+2}{3}\vec{E}_e \tag{5.1}$$

which then, with the same calculation for the avearge orientation of the dipoles leads to the expression:

$$\frac{\epsilon-1}{\epsilon+2} = \frac{\rho\mu^2}{9\epsilon_0 k_B T} + \frac{\rho\alpha}{3\epsilon_0} \tag{5.2}$$

or, with the introduction of the high frequency dielctric constant, for which a similar argument can be used:

$$\frac{\epsilon-1}{\epsilon+2} - \frac{\epsilon_\infty-1}{\epsilon_\infty+2} = \frac{\rho\mu^2}{9\epsilon_0 k_B T} \tag{5.3}$$

Debye then continues to show that for a number of substances the graph of the function $(\epsilon-1)T/(\epsilon+2)$ *vs* T is indeed a straight line.

The internal field according to Lorentz.

Lorentz [4] gives a derivation of the internal field which we will quote entirely adapting the notation at various places, as to conform with the notation introduced here.

> We shall observe in the first place that the field in the immediate neighborhood of a polarized particle may be determined by the laws of electrostatics, even when the electric moment is not constant. Take, for instance, the case treated in § 43 (this paragraph treats dipole radiation). It was stated in note 23 that at great distances the terms resulting from the differentiation of the goniometric function are very much greater than those which arise from the differentiation of $\frac{1}{r}$. These latter, on the contrary, predominate when we confine ourselves to distances that are very small compared to the wavelength; then we may write (for the potentials of the time dependent dipole $\vec{p}$):
>
> $$\phi = -\frac{1}{4\pi\epsilon_0}\vec{p}\cdot\vec{\nabla}\frac{1}{r}, \quad \text{and} \quad \vec{a} = 0 \tag{1}$$
>
> from which it appears that the field is identical with the electrostatic field that would exist, if the moment $\vec{p}$ were kept constant.

It is further to be noted that the difference between the mean electric force and the electric force existing in a small cavity depends only on the actions going on at very small distances, so that we may deal with this difference as if we had to do with an electrostic system.

Let us therefore consider a system of molecules with invariable electric moments and go into some details concerning the electric force existing in it.

The field produced by the electrons being determined by

$$\Delta\phi = -\frac{\rho}{\epsilon_0}, \quad \text{and} \quad \vec{e} = -\vec{\nabla}\phi \tag{2}$$

we have for the mean values

$$\Delta\overline{\phi} = -\frac{\overline{\rho}}{\epsilon_0}, \quad \text{and} \quad \vec{E} = \overline{\vec{e}} = -\vec{\nabla}\overline{\phi} \tag{3}$$

or, in words: the mean electric force is equal to the force that would be produced by a charge distributed with the mean or, let us say, the "effective" density $\overline{\rho}$.

In the definition of a mean value $\overline{\phi}$ given in §113 it was expressly stated that the space **S** was of spherical form. It is easily seen, however, that we may as well give it any shape we like, provided it be infinitely small in a physical sense. The equation

$$\overline{\rho}\mathbf{S} = \int \rho\, dS \tag{4}$$

may therefore be interpreted by saying that for any space of the said kind the effective charge (meaning by these words the product of $\overline{\phi}$ and **S**) is equal to the total real charge.

We shall now examine the distribution of the effective charge. Suppose, for the sake of simplicity, that a molecule contains two electrons situated at the points A and B with charges $-e$ and $+e$, (?) and denote by $\vec{r}$ the vector AB. There will be as many of these vectors, of different directions and lengths, as there are molecules. Now, if the length of these vectors is much greater than the size of the electrons, we may neglect the intersections of the bounding surfaces of the space **S** with the electrons themselves, but there will be a great number of intersections with the lines AB. These may not be left out of account, because for any complete molecule $\int \rho dS = 0$, whereas each of the said intersections contributes to the effective charge within σ (the bounding surface of **S**) by an amount $-e$ or $+e$ as $\vec{r}\cdot\vec{n}$ (where $\vec{n}$ is the normal to σ drawn outwards) is positive or negative. Hence the total charge within σ may be represented by a surface integral. In order to find the part of it corresponding to an element $d\sigma$ (infinitely small in a physical sense) we begin by fixing our attention on those among the lines AB which have some definite direction and some definite length. If the starting points A are iregularly distributed and if, for the group considerd, there

number per unit volume is ν, the number of interseections with $d\sigma$ will be $\nu\vec{r}\cdot\vec{n}d\sigma$ when $\vec{r}\cdot\vec{n}$ is positive, and $-\nu\vec{r}\cdot\vec{n}d\sigma$ when it is negative. Therefore, the part contributed to the charge within σ is $-\nu e\vec{r}\cdot\vec{n}d\sigma$ in both cases, and the total part associated with $d\sigma$ is $-\sum\nu\vec{r}\cdot\vec{n}d\sigma$, the sum being extended to all the groups of lines AB. But $e\vec{r}$ is the electric moment of a particle, $\nu e\vec{r}$ the moment per unit of volume of the chosen group, and $\sum\nu e\vec{r}$ the total moment per unit of volume. Denoting this by $\vec{P}$, we have for the above expression $-\sum\nu e\vec{r}\cdot\vec{n}$ the value $-\vec{P}\cdot\vec{n}$, and for the effective charge enclosed by the surface σ

$$-\int\vec{P}\cdot\vec{n}\,d\sigma \tag{5}$$

As the difference between $\vec{E}$ and the electric force in a cavity depends exclusively on the state of the system in the immediate vicinity of the point considered, we may now conceive the polarization $\vec{P}$ to be uniform. In this case the above integral is zero for any closed surface lying interely within the body, so that the effective charge may be said to have its seat on the bounding surface Σ. Its surface density is found by calculating the above integral for the surface of a flat cylinder, the two plane sides of which are on both sides of an element $d\Sigma$ at a distance from each other that is infinitely small in comparison with the dimensions of $d\Sigma$. Calling $\vec{N}$ the normal to the surface Σ, we have at the outer plane $\vec{P}\cdot\vec{n}=0$ (if we suppose the body to be surrounded by ether), and at the inner one $\vec{P}\cdot\vec{n}=-\vec{P}\cdot\vec{N}$. The amount of effective charge contained in the cylinder is therefore given by $\vec{P}\cdot\vec{N}d\Sigma$, and the charge may be said to be distributed over the surface with a density $\vec{P}\cdot\vec{N}$.

Now consider a point A of the body. By what has been said, the electric force $\vec{E}$ at this point is due to the charge $\vec{P}\cdot\vec{N}$ on the bounding surface Σ. If, however, a spherical cavity is made around A as center, there will be at this point an additional electrioc force $\vec{E}'$, caused by a similar charge on the walls of the cavity, and obviously having the direction of $\vec{P}$. The magnitude of this force is found as follows. Let a be the radius of the sphere, $d\sigma$ an element of its surface, ϑ the angle between the radius drawn towards this element and the polarization $\vec{P}$. The surface density on $d\sigma$ being $-P\cos\vartheta$, we have for the force produced at A

$$\frac{1}{4\pi a^2}\int P\cos^2\vartheta\,d\sigma \tag{6}$$

giving

$$\vec{E}'=\frac{1}{3}\vec{P} \tag{7}$$

Our foregoing remarks show that the expression

$$\vec{E}+\frac{1}{3}\vec{P} \tag{8}$$

may always be used for the electric force at the center of a spherical cavity, even though the polarization of the body change from point to point and from one instant to the next.

The reasoning for getting eq. (6) is rather unclear to me.
The previous quote shows that Lorentz attributes the field in the cavity to the surface charge on a spherical cavity. Let's try a different derivation. Suppose the polarization in the medium is given by $\vec{P}(\vec{r})$. The potential at any point is then given by the integral equation:

$$\phi(\vec{r}) = -\frac{1}{4\pi\epsilon_0}\int d\vec{r}\,' \frac{\vec{\nabla}' \cdot \vec{P}(\vec{r}\,')}{|\vec{r} - \vec{r}\,'|} \tag{5.4}$$

This integral is over all space, and in view of the discontinuity in $\vec{P}$ at the surface of the cavity, the divergence has a delta function, and we have to be careful evaluating this integral. This can be converted to a surface integral in the following way: first we write:

$$\phi(\vec{r}) = -\frac{1}{4\pi\epsilon_0}\int d\vec{r}\,' \left(\vec{\nabla}' \cdot \frac{\vec{P}(\vec{r}\,')}{|\vec{r} - \vec{r}\,'|} - \vec{P}(\vec{r}\,') \cdot \vec{\nabla}' \frac{1}{|\vec{r} - \vec{r}\,'|} \right) \tag{5.5}$$

We can now use Gauss' theorem to rewrite the first term as a surface integral:

$$\phi(\vec{r}) = \frac{1}{4\pi\epsilon_0}\int_S d\vec{s}\,' \frac{\vec{n}\,' \cdot \vec{P}(\vec{r}\,')}{|\vec{r} - \vec{r}\,'|} - \frac{1}{4\pi\epsilon_0}\vec{\nabla} \cdot \int_V d\vec{r}\,' \frac{\vec{P}(\vec{r}\,')}{|\vec{r} - \vec{r}\,'|} \tag{5.6}$$

Note that the volume is outside the cavity, so the normal points "inwards".
In the second integral there is now no problem taking $\vec{P}$ as a constant, since that does no longer lead to singularities.
Putting $\vec{P}$ a constant everywhere then yields:

$$\phi(\vec{r}) = \frac{1}{4\pi\epsilon_0}\vec{P} \cdot \int_S d\vec{s}\,' \frac{\vec{n}\,'}{|\vec{r} - \vec{r}\,'|} - \frac{1}{4\pi\epsilon_0}\vec{P} \cdot \vec{\nabla} \int_V d\vec{r}\,' \frac{1}{|\vec{r} - \vec{r}\,'|} \tag{5.7}$$

We want to caluculate the electric field, so we take the gradient, and we want it at the center of the cavity, so we put $\vec{r} = 0$, but after taking the gradients. This leads to the expression:

$$\vec{E} = -\left(\vec{\nabla}\phi(\vec{r})\right)_{r=0} = \frac{1}{4\pi\epsilon_0 a^2}\vec{P} \cdot \int_S d\vec{s}\,'\vec{n}\,'\vec{n}\,' + \frac{1}{4\pi\epsilon_0}\vec{P} \cdot \int_V d\vec{r}\,'\vec{\nabla}'\vec{\nabla}'\frac{1}{r'} \tag{5.8}$$

where the second integral gives 0, for the same reasons as were explained in section 2. The first integral gives $\frac{4\pi}{3}a^2$, so that

$$\vec{E}_P = \frac{1}{3\epsilon_0}\vec{P} \tag{5.9}$$

is the electric field at the origin of the cavity due to the polarization. This is exactly Lorentz' result. The implication is that the effect of the boundary is partially taken into account. In fact one should solve the boundary value problem first, and then calculate the internal field with the above integral.
In this context: see also Lorentz[4], §117, and Fröhlich[2], p. 22.

6 Dielectric constant according to Onsager.

Next we come to Onsager's treatment of the dielectric constant. Onsager [5] goes into considerable more detail, which will be outlined in this section.
His major critique is that Debye uses the total internal field to orient the molecule, whereas according to his way of thinking about it, only part of this field should be used, namely that part which does not depend on the original dipole itself (and which of course contributes to the polarization). So he needs to calculate two fields: the field due to the dielectric outside the cavity, and the reaction field due to the dipole inside the cavity. His starting point is that the Clausius–Mosotti (or Debye) expression eq. (6.2) leads to a phase transition for the polarization, namely for a certain critical temperature T_c, ϵ goes to ∞, which is only very rarely obeserved, but it also means that fluids with high dielectric constants are necessarily close to this phase transition, and should therefore exhibit large (critical) fluctuations. This is also not observed.
The first step is to derive the reaction field of a dipole at the center of a spherical cavity, again with radius a.
The solutions for the inside– and outside electric fields due to such a dipole $\vec{\mu}$ can be written as

$$\vec{E}_{\rm i} = \frac{1}{4\pi\epsilon_0 r^3}\vec{\mu}\cdot(\mathbf{1} - 3\hat{r}\hat{r}) - \vec{R} \tag{6.1}$$

where the *reaction field* $\vec{R}$ is given by:

$$\vec{R} = \frac{1}{4\pi\epsilon_0 a^3}\frac{2(\epsilon-1)}{2\epsilon+1}\vec{\mu} \tag{6.2}$$

and

$$\vec{E}_{\rm out} = \frac{1}{4\pi\epsilon_0\epsilon r^3}\vec{\mu}^*\cdot(\mathbf{1} - 3\hat{r}\hat{r}) \tag{6.3}$$

where the *external moment* $\vec{\mu}^*$ is given by

$$\vec{\mu}^* = \frac{3\epsilon}{2\epsilon+1}\vec{\mu} \tag{6.4}$$

The second boundary value problem that has to be solved is the one alluded to at the end of the previous section, namely that of an empty cavity, embedded in a dielectric in which a constant electric field $\vec{E}$ is present. This boundary value problem leads to the following expressions for internal and external fields:

$$\vec{E}_{\rm in} = \vec{G} = \frac{3\epsilon}{2\epsilon+1}\vec{E} \tag{6.5}$$

and

$$\vec{E}_{\rm out} = \frac{\epsilon-1}{2\epsilon+1}\frac{a^3}{r^3}\vec{E}\cdot(\mathbf{1} - 3\hat{r}\hat{r}) + \vec{E} \tag{6.6}$$

The total field acting on the dipole in a spherical cavity is therefore

$$\vec{F} = \vec{G} + \vec{R} = \frac{3\epsilon}{2\epsilon+1}\vec{E} + \frac{2(\epsilon-1)}{4\pi\epsilon_0 a^3(2\epsilon+1)}\vec{\mu} \tag{6.7}$$

and the dipole moment of the molecule is given by

$$\vec{\mu} = \vec{\mu}_0 + \alpha\vec{F} \tag{6.8}$$

where $\vec{\mu}_0$ is the permament dipole moment of the molecule in the absence of external fields. Furthermore we can introduce the refractive index n through the relation

$$\frac{\alpha}{4\pi\epsilon_0 a^3} = \frac{3}{4\pi a^3\rho}\frac{n^2-1}{n^2+2} \approx \frac{n^2-1}{n^2+2} \tag{6.9}$$

With this relation it is easy to derive from eqs. (7.7) and (7.8) the dipole moment of the molecule:

$$\vec{\mu} = \frac{(2\epsilon+1)(n^2+2)}{3(2\epsilon+n^2)}\vec{\mu}_0 + \frac{\epsilon(n^2-1)}{2\epsilon+n^2}4\pi\epsilon_0 a^3\vec{E} \tag{6.10}$$

The next step in Onsager's calculation is establishing the potential of mean torque. He gives two methods, of which we will only give the first. The basic problem is that the reaction field should not contribute to the torque on the dipole since it is in the direction of the dipole moment. The situation is made complicated by the polarizability. But it is fairly simple to calculate the torque on the dipole $\vec{\mu}$, which is of course given by:

$$\vec{M} = \vec{F} \times \vec{\mu} \tag{6.11}$$

and subsequently find the potential which will give rise to this torque. (NB. compare to free energy calculations).
A direct calculation shows that

$$\vec{F} \times \vec{\mu} = \frac{3\epsilon}{2\epsilon+1}\vec{E} \times \vec{\mu} = \vec{E} \times \vec{\mu}^* \tag{6.12}$$

We note, however, that the part of $\vec{\mu}$ proportional to $\vec{E}$ does not contribute to the torque, and by inserting (7.10) we obtain:

$$\vec{M} = \frac{\epsilon(n^2+2)}{2\epsilon+n^2}\vec{E} \times \vec{\mu}_0 \tag{6.13}$$

so that

$$\vec{\mu}_0^* = \frac{\epsilon(n^2+2)}{2\epsilon+n^2}\vec{\mu}_0 \tag{6.14}$$

This means that the potential of mean torque is given by

$$w = -\vec{\mu}_0^* \cdot \vec{E} \tag{6.15}$$

which is the potential that has to be substituted in the Boltzmann factor. We note here that, if the polarizability is neglected, this is just the internal field, but now solved with the correct boundary condition, whereas Lorentz did not bother to solve the boundary value problem, just took the polarization constant everywhere.
This allows us to calculate $\left\langle \vec{\mu} \cdot \hat{E} \right\rangle$. Using (7.10) we get:

$$\left\langle \vec{\mu} \cdot \hat{E} \right\rangle = \frac{2\epsilon+1}{3\epsilon}\left\langle \vec{\mu}_0^* \cdot \hat{E} \right\rangle + \frac{\epsilon(n^2-1)}{2\epsilon+n^2}4\pi\epsilon_0 a^3 E \tag{6.16}$$

and with (7.15) it is easy to see that (see also the calculation leading to (2.3)):

$$\left\langle \vec{\mu}_0^* \cdot \hat{E} \right\rangle = \frac{(\mu_0^*)^2 E}{3k_B T} \tag{6.17}$$

Using this we find for the polarization in the medium the following expression:

$$\vec{P} = \rho \left(\frac{\epsilon(n^2+2)^2(2\epsilon+1)}{(2\epsilon+n^2)^2} \frac{\mu_0^2}{9k_B T} + \frac{\epsilon(n^2+2)}{2\epsilon+n^2}\alpha \right) \vec{E} \tag{6.18}$$

We therefore find for the dielectric constant the following consistency relation:

$$\epsilon_0(\epsilon - 1) = \rho \left(\frac{\epsilon(n^2+2)^2(2\epsilon+1)}{(2\epsilon+n^2)^2} \frac{\mu_0^2}{9k_B T} + \frac{\epsilon(n^2+2)}{2\epsilon+n^2}\alpha \right) \tag{6.19}$$

Again a strightforward calculation then yields the following relation:

$$\frac{(2\epsilon+n^2)(\epsilon-n^2)}{\epsilon(n^2+2)^2} = \frac{\rho\mu_0^2}{9\epsilon_0 k_B T} \tag{6.20}$$

It is to be noted here that for the polarizability part, the Clausius–Mosotti relation is again used, which seems strange, since the internal field for the derivation of Clausius–Mosotti is the Lorentz cavity field, and not the internal field found by solving the boundary value problem.
This ends our exposure of Onsager's theory. He has a few more things to say, especially about mixtures, but these are not of immediate interest to us here. At the end of this section we also note that so far all theories are macroscopic, and basically try to derive expressions for the dielectic constant using consistency arguments. This will change in the next sections, where we start out from fundamental statistical mechanics considerations.

7 Dielectric constant according to Kirkwood.

In this section we outline the theory of dielectric polarization of Kirkwood [6]. Kirkwood's generalization is an extension of Onsager to take better into account the local correlations. A quote from Kirkwood reads:

> The most serious defect of the model lies in the assumption of a uniform local dielectric constant, identical with the macroscopic dielectric constant of the medium. Moreover, the hindered rotation of the neighbors of a molecule, relative to itself, which is implicit in the deviation of the local from the average polarization, is attributed entirely to the dipole field of the central molecule.

We read this to mean that the reaction field, as calculated by Onsager is inadequate, since in the immediate neighborhood of the central molecule (cavity), due to for instance large electric fields the dielectric behavior is not equal to the bulk dielectric behavior, and secondly that short range molecular forces can also be of importance in determining the average orientation of a molecule close to the central molecule.

Starting point of Kirkwood's derivation is the classical statistical mechanical equilibrium partition function of a collection of dipoles in an external field. The total electric moment $\vec{M}$ is the vector sum of the molecular dipole moments $\vec{\mu}_i$:

$$\vec{M} = \sum_{i=1}^{N} \vec{\mu}_i \tag{7.1}$$

and the average dipole moment component of molecule i in the direction of the field $\hat{E}$, denoted by $\left\langle \vec{\mu}_i \cdot \hat{E} \right\rangle_E$ is defined as:

$$\left\langle \vec{\mu}_i \cdot \hat{E} \right\rangle_E = \frac{\int d\Gamma \, \vec{\mu}_i \cdot \hat{E} e^{-\beta(V_N - \vec{M}\cdot\vec{E}_0)}}{\int d\Gamma \, e^{-\beta(V_N - \vec{M}\cdot\vec{E}_0)}} \tag{7.2}$$

where V_N is the total N–particle interaction potential (including short range and dipolar interactions), and $d\Gamma$ a phase space element.
Expansion in powers of the electric field then yields to lowest order:

$$\left\langle \vec{\mu}_i \cdot \hat{E} \right\rangle_E = \beta \left\langle (\vec{\mu}_i \cdot \hat{E})(\vec{M} \cdot \hat{E}) \right\rangle E_0 \tag{7.3}$$

where the average on the right hand side is now to be calculated in the absence of of an external field.
Next Kirkwood assumes that the internal field can be related to the external field by the relation

$$\vec{E} = \frac{3}{\epsilon + 2} \vec{E}_0 \tag{7.4}$$

which means that he takes a spherical dielectric medium and shoves it into the external field; secondly, using isotropy of the system in the absence of external field, we can write

$$\left\langle \vec{\mu}_i \cdot \hat{E} \right\rangle_E = \frac{\epsilon + 2}{3} \frac{1}{3k_B T} \left\langle \vec{\mu}_i \cdot \vec{M} \right\rangle E \tag{7.5}$$

The remaining average is performed in two steps: first over all configurations for *given* $\vec{\mu}_i$, and subsequently over all orientations of $\vec{\mu}_i$. Since the averages are performed in the absence of fields, this last step is irrelevant. Thus we find:

$$\left\langle \vec{\mu}_i \cdot \vec{M} \right\rangle = \left\langle \vec{\mu}_i \cdot \overline{\vec{M}}_i \right\rangle = \vec{\mu} \cdot \overline{\vec{M}} \tag{7.6}$$

In this expression $\overline{\vec{M}}_i$ is the average of $\vec{M}$ for given $\vec{\mu}_i$, and in the final step we used that this average must be the same for all molecules, so the index can be dropped.
This all leads to the Clausius–Mosotti type expression

$$\frac{\epsilon - 1}{\epsilon + 2} = \frac{\rho \vec{\mu} \cdot \overline{\vec{M}}}{9\epsilon_0 k_B T} \tag{7.7}$$

which indeed reduces to Clausius–Mosotti if for $\overline{\vec{M}}$ we substitute $\vec{\mu}$, in other words if we take all dipoles to be uncorrelated, except for the central dipole itself of course. Also Onsager should result if the correlation is given by just the reaction field.

Using the results of appendix A, we derive for the correlation:

$$\vec{\mu} \cdot \overline{\vec{M}} = \frac{9\epsilon}{(\epsilon+2)(2\epsilon+1)}\mu^2 \tag{7.8}$$

Introducing this into eq. (8.7) yields:

$$\frac{(2\epsilon+1)(\epsilon-1)}{\epsilon} = \frac{\rho\mu^2}{\epsilon_0 k_B T} \tag{7.9}$$

which is indeed eq. (7.20) with $n^2 = 1$.
Kirkwood goes one step beyond this result, by taking local correlation effects into account. The above derivation of Onsager's result shows that Onsager takes at least part of this correlation into account, namely the reaction field, but according to Kirkwood this is not sufficient. (see the above quote).
Kirkwood's improvement consists of the fact that rather than directly using eq. (A.8) he states that this result is in fact only valid if no short range contributions to the interaction potential, and no saturation effects are important.
He derives the following expression:

$$\frac{(2\epsilon+1)(\epsilon-1)}{\epsilon} = \frac{\rho\vec{\mu} \cdot \overline{\vec{\mu}}}{\epsilon_0 k_B T} \tag{7.10}$$

where $\overline{\vec{\mu}}$ now contains the effect of short range correlations. An explicit expression is given for the case where there is a rather welll defined rigid solvation shell around the central dipole:

$$\vec{\mu} \cdot \overline{\vec{\mu}} = \mu^2(1 + z\,\langle\cos\gamma\rangle) \tag{7.11}$$

where the solvation number is z and $\langle\cos\gamma\rangle$ is the average orientation between two dipoles.

8 Dielectric constant according to Cole.

One thing missing in Kirkwood's derivation is the effect of polarizability, although at various places (for instance the calculation of the central dipole moment) it is taken into account on an *ad hoc* basis. Cole [7] tries to improve on that on the basis of a simple harmonic oscillator model. Apparently a number of attempts were made to include polarizability directly, leading to different expresions, but they missed the consistency of Onsager's approach. (See other entries in te literature list). The main problem appears to be that calculation of the polarization for given central dipole on the basis of statistical mechanics leads to a conceptual problem, in that the dipole moment of a polarizable dipole cannot be fixed without fixing the electric field, meaning the dipole moments of all the other dipoles, and this is not necessarily an equilibrium configuration. Cole gets around this problem by explicitly taking the internal coordinate into account, albeit in the harmonic oscillator approximation.
So, Cole's starting point is the interaction Hamiltonian:

$$\mathcal{H} = U_s + \frac{1}{2}\sum_i k_i \vec{r}_i^{\,2} + \frac{1}{2}\sum_{i\neq j}(\vec{\mu}_{0i} + e_i\vec{r}_i) \cdot \mathrm{T}_{ij} \cdot (\vec{\mu}_{0j} + e_j\vec{r}_j) - \sum_i (\vec{\mu}_{0i} + e_i\vec{r}_i) \cdot \vec{E}_0 \tag{8.1}$$

where U_s is a short range interaction energy between the molecules which is not further specified, $\vec{r}_i$ is an internal coordinate, which oscillates harmonically with spring constant k_i; $\vec{\mu}_{0i}$ is the permanent dipole moment of molecule i, and $e_i\vec{r}_i$ the induced moment, so that the third term represents the dipole–dipole interaction, T_{ij} being the dipole tensor, and the last term is the dipole interaction energy with an external field. Finally the tensor T is given by

$$\mathrm{T}_{ij} = \frac{1}{4\pi\epsilon_0 R_{ij}^3}\left(\mathbf{1} - 3\hat{R}_{ij}\hat{R}_{ij}\right) \tag{8.2}$$

where $\vec{R}_{ij}$ denotes the connecting vector between the particles i and j.
The force on the coordinate $\vec{r}_i$ is for a given field $\vec{E}_0$ given by

$$k_i\vec{r}_i + e_i\sum_{j\neq i}\mathrm{T}_{ij} \tag{8.3}$$

where we only took the dipolar part due to the other polarizabilities, not due to the permanent dipoles. Supposedly this is done in van Vleck, but so far I have not seen that.
The equilibrium value for the $\vec{r}_i$, $\vec{r}_{Ei}$, in the presence of an external field is given by

9 Final remarks.

1. This is something I don't understand: take the refractive index in the Onsager derivation equal to 1. In that case the potential of mean force: eq. (7.15) is given by:

$$w = -\frac{3\epsilon}{2\epsilon+1}\vec{\mu}_0\cdot\vec{E} = -\vec{\mu}_0\cdot\vec{E}_{\mathrm{in}} \tag{9.1}$$

and the reason is that the internal field is now calculated from a boundary value problem, *cf.* eq. (7.5).

This implies that the desired average is given by:

$$\left\langle\vec{\mu}\cdot\hat{E}\right\rangle = \frac{3\epsilon}{2\epsilon+1}\frac{\mu_0^2}{3k_BT}E \tag{9.2}$$

so that the polarization becomes:

$$\vec{P} = \frac{\rho\epsilon\mu_0^2}{(2\epsilon+1)k_BT}\vec{E} \tag{9.3}$$

which leads to

$$\frac{(2\epsilon+1)(\epsilon-1)}{\epsilon} = \frac{\rho\mu_0^2}{\epsilon_0 k_BT} \tag{9.4}$$

which is again eq. (7.20) with $n^2 = 1$.

The point we can make here is the following: it is only the internal field that is changed from the Lorentz field, $\frac{1}{3}(\epsilon+2)\vec{E}$ to the internal cavity field $\frac{3\epsilon}{2\epsilon+1}\vec{E}$. No reaction field part enters here.

On the other hand, however, we have shown that Kirkwood's method, combined with the dipolar reaction field as the correlation between the central dipole and the other dipoles leads to exactly the same result. Here we do not have to calculate the internal field, only correlation functions in the absence of a field. Somehow this correlation appears to be missing from Onsager's work.

It could be a coincidence based on a relation Onsager points out between on the one hand the internal field G and E, eq. (7.5), which yields

$$\frac{G}{E} = \frac{3\epsilon}{2\epsilon + 1} \tag{9.5}$$

and on the other hand the relation between external dipole moment and vacuum dipole moment

$$\frac{\mu*}{\mu} = \frac{3\epsilon}{2\epsilon + 1} \tag{9.6}$$

which are exactly the same.

(Side remark: maybe worth looking into in the case of quadrupolar dielectrics?).

2. In general Clausius–Mosotti is considered a good expression for gases, or for polarizable media with no permanent dipole moments on the molecules. Nevertheless it is not true that if we let the density in Onsager's expression, which, with Kirkwoods modification, is considered good for polar media, become small, we get Clausius–Mosotti back. This fact is probably related to something else: if we solve the boundary value problems, and finally let the cavity radius go to zero, we get a different result than for the case where we begin with no cavity at all. If we have no cavity at all, the internal field can be written as:

$$\vec{E}_{\text{in}} = \frac{1}{\epsilon}\vec{E} \tag{9.7}$$

which leads to:

$$\epsilon(\epsilon - 1) = \frac{\rho\mu_0^2}{3\epsilon_0 k_B T} \tag{9.8}$$

an expression I have never encountered.

In addition, for polarizable media it could be argued that the cavity is filled with the same polarizable molecule that the fluid consists of, so that (10.7) would indeed be a better expression for the internal field. For polarizable media we would then get

$$\epsilon_\infty(\epsilon_\infty - 1) = \frac{\rho\alpha}{\epsilon_0} \tag{9.9}$$

In this context, van Vleck [8] claims the following

> Our method of partition functions is to be contrasted with the usual, essentially static Lorentz method of representing dipole–dipole coupling by a local field $(\cdots)$ for a long test body. The Lorentz procedure is shown to be only a first approximation, which is really warranted if the density is so low, or the temperature so high that one may neglect all terms but the first in the development of the partition function in $1/T$.

The question arises if the boundary conditions need modification in the case of low density, and if so, how? Look into the development of hydrodynamic boundary conditions?

See in this context also appendix C.

3. Consistency.

Another thing that is slightly mysterious is the following: To calculate the relation between polarizability, the simplest model is just to take the induced dipole moment proportional to the vacuum field, and the susceptibility the relation between the polarization and the vacuum field: for a gas of polariable non–dipolar molecules we then get (*cf.* eq. (3.3))

$$\epsilon_\infty - 1 = \frac{\rho_0 \alpha}{\epsilon_0} \tag{9.10}$$

This seems consistent. The next level of refinement is to take the Lorentz field as the field acting on the molecule, thus inducing polarization, which leads to Clausius–Mosotti: (*cf.* eq. (5.3))

$$\frac{\epsilon_\infty - 1}{\epsilon_\infty + 2} = \frac{\rho_0 \alpha}{3\epsilon_0} \tag{9.11}$$

This seems somehow inconsistent, in that the susceptibility is now taken to be the proportionality factor with the vacuum field, whereas it should be the prportionality factor to the internal field. If we do that, however, of course eq. (9.10) would be recovered.

Now the next level of refinement would be to use the Onsager cavity field for the internal field. In that case we would find, by the same (inconstent?) procedure:

$$\frac{(2\epsilon_\infty + 1)(\epsilon_\infty - 1)}{3\epsilon_\infty} = \frac{\rho_0 \alpha}{\epsilon_0} \tag{9.12}$$

which is not what Onsager uses for the high polarizability, in stead he uses Clausius–Mosotti, which seems even more inconsistent.

The results of appendix C, however, show the correctness of Clausius –Mosotti for low densities, or whatever the exact expansion parameter is in that procedure.

We can also look at the expansion of ϵ_∞ as a function of $x = \rho_0 \alpha / \epsilon_0$ for the various cases: Eq. (9.10) obviously leads to:

$$\epsilon_\infty^0 = 1 + x \tag{9.13}$$

Expansion of the Clausius–Mosotti function eq. (9.11) gives:

$$\epsilon_\infty^{\mathrm{CM}} = 1 + x + \frac{1}{3}x^2 + \frac{1}{9}x^3 \cdots \tag{9.14}$$

and finally Onsager (9.12) also yields

$$\epsilon_\infty^{\mathrm{Ons}} = 1 + x + \frac{1}{3}x^2 - \frac{1}{9}x^3 + \cdots \tag{9.15}$$

which shows that Onsager and Clausius–Mosotti agree up to second order in the expansion parameter.

4. Correlations.

In the Lorentz model, there are no correlations between the existence of a hole and the polarization field outside. Still there is an internal field different from the external field. In the Onsager model, the presence of the hole causes the polarization to be modified. The hole "creates " a dipolar polarization field around it, and this dipolar field again leads to the modification of the inside field. We can therefore view the difference between the Lorentz and the Onsager field inside as a correlation effect:

$$\vec{E}_{\text{in}}^{\text{Ons}} - \vec{E}_{\text{in}}^{\text{L}} = \frac{8\epsilon - 2}{3(2\epsilon + 1)}\vec{E} \tag{9.16}$$

It seems to me that this must be sort of a maximum. For low densities, the system does not even realize there is a hole, the distances between the molecules are such that holes the size of the particle radius are constantly present. The other extreme is that the distances between the molecules are so small that all space is filled with dielctric. So why doesn't the density enter into this part of the picture?

Now here is something I had not realized before. Lorentz also neglects the correlations between the existence of a central dipole and the outside polarization. Onsager puts a polarizable dipole in the cavity, this dipole polarizes the surrounding and therefore causes a reaction field which again acts on the dipole, thus enlarging it. Calculation of this effect, gives an additional contribution to the internal electric field. This can be seen as follows: The dipole moment is proportional to the total internal electric field:

$$\vec{\mu} = \alpha\left(\vec{E}_{\text{in}} + \vec{R}\right) \tag{9.17}$$

The reaction field $\vec{R}$ is given by eq. (6.2):

$$\vec{R} = \frac{1}{4\pi\epsilon_0 a^3}\frac{2(\epsilon - 1)}{2\epsilon + 1}\vec{\mu} \tag{9.18}$$

Combining these last two equations the gives:

$$\vec{R} = \frac{1}{4\pi\epsilon_0 a^3}\frac{2(\epsilon - 1)}{2\epsilon + 1}\alpha\left(\vec{E}_{\text{in}} + \vec{R}\right) \tag{9.19}$$

or,

$$\vec{R} = \left(1 - \frac{\alpha}{4\pi\epsilon_0 a^3}\frac{2(\epsilon - 1)}{2\epsilon + 1}\right)^{-1}\frac{\alpha}{4\pi\epsilon_0 a^3}\frac{2(\epsilon - 1)}{2\epsilon + 1}\vec{E}_{\text{in}} \tag{9.20}$$

and hence

$$\vec{E}_{\text{in}} + \vec{R} = \left(1 - \frac{\alpha}{4\pi\epsilon_0 a^3}\frac{2(\epsilon - 1)}{2\epsilon + 1}\right)^{-1}\frac{3\epsilon}{2\epsilon + 1}\vec{E} \tag{9.21}$$

If we now assume that the density is related to the radius by

$$\rho^{-1} = \frac{4}{3}\pi a^3 \tag{9.22}$$

and using that $\vec{P} = \rho\alpha = \epsilon_0(\epsilon - 1)\vec{E}$ we then find the following relation

$$\frac{3\epsilon\rho\alpha}{2\epsilon + 1 - \frac{2\rho\alpha}{3\epsilon_0}(\epsilon - 1)} = \epsilon_0(\epsilon - 1) \tag{9.23}$$

from which we again find Clausius–Mosotti. So the remark made under the previuos note that there is an additional inconsitency in Onsager is in fact incorrect.

Yet another way of looking at this is that the combined effect of the hole–polarization correlation, and the reaction field business again yields the Lorentz field [2]. Using Clausius–Mosotti to eliminate $\rho\alpha$ in (9.21) we find after some simple calculations:

$$\vec{E}_{\text{in}} + \vec{R} = \frac{\epsilon + 2}{3}\vec{E} \tag{9.24}$$

which is indeed the Lorentz field.

The areas of application are different: Lorentz is supposed to hold for low density gases, whereas for Onsager (9.22) has to be used, which is in fact a condition for all space to be completed filled with spheres. Another coincidence with which this whole field abounds.

A Dipole in a cavity at the centre of a dielectric sphere.

Consider the situation where we have a spherical cavity at the centre of a dielectric sphere. The radius of the cavity is assumed to be a, and of the sphere it is given by R. We have potentials in three different regions, given respectively by

$$\psi_1 = \frac{\vec{\mu}\cdot\vec{r}}{4\pi\epsilon_0 r^3} + A\vec{\mu}\cdot\vec{r}, \quad \text{for} \quad r < a \tag{A.25}$$

in the core region,

$$\psi_2 = B\frac{\vec{\mu}\cdot\vec{r}}{4\pi\epsilon_0 r^3} + C\vec{\mu}\cdot\vec{r}, \quad \text{for} \quad a < r < R \tag{A.26}$$

in the intermediate region, and finally

$$\psi_3 = D\frac{\vec{\mu}\cdot\vec{r}}{4\pi\epsilon_0 r^3}, \quad \text{for} \quad r > R \tag{A.27}$$

The boundary conditions determine the values of the four coefficients. The relations between the coefficients are:

$$\begin{aligned} 4\pi\epsilon_0 a^3 A - B - 4\pi\epsilon_0 a^3 C &= -1 \\ 4\pi\epsilon_0 a^3 A + 2\epsilon B - 4\pi\epsilon_0\epsilon a^3 C &= 2 \\ B + 4\pi\epsilon_0 R^3 C - D &= 0 \\ -2\epsilon B + 4\pi\epsilon_0\epsilon R^3 C + 2D &= 0 \end{aligned} \tag{A.28}$$

The solutions for the coefficients are:

$$\begin{aligned} 4\pi\epsilon_0 a^3 A &= \frac{2(1-\epsilon) + 2\epsilon\frac{a^3}{R^3}\frac{\epsilon-1}{\epsilon+2}}{2\epsilon + 1 - 2\frac{a^3}{R^3}\frac{(\epsilon-1)^2}{\epsilon+2}} \\ B &= \frac{3}{2\epsilon + 1 - 2\frac{a^3}{R^3}\frac{(\epsilon-1)^2}{\epsilon+2}} \\ 4\pi\epsilon_0 R^3 C &= \frac{2(\epsilon-1)}{\epsilon+2}B \\ D &= \frac{3\epsilon}{\epsilon+2}B \end{aligned} \tag{A.29}$$

To calculate the necessary integral we need the polarization in the dielectric medium, which is given by:

$$\vec{P} = -\epsilon_0(\epsilon-1)\vec{\nabla}\psi_2 = -\frac{B(\epsilon-1)}{4\pi r^3}\vec{\mu}\cdot(1 - 3\hat{r}\hat{r}) - \epsilon_0(\epsilon-1)C\vec{\mu} \tag{A.30}$$

In the integration over the medium the first term again cancels in view of the symmetry, and we find:

$$\int d\vec{r}\,\vec{P} = -\epsilon_0(\epsilon-1)\vec{\mu}C\int_{r=a}^{r=R} d\vec{r} = -\frac{4\pi}{3}\epsilon_0(\epsilon-1)\vec{\mu}CR^3\left(1 - \frac{a^3}{R^3}\right) \tag{A.31}$$

In the limit $R \rightarrow \infty$ this becomes:

$$\lim_{R\to\infty} \int d\vec{r}\, \vec{P} = -\frac{2(\epsilon-1)^2}{(\epsilon+2)(2\epsilon+1)}\vec{\mu} \tag{A.32}$$

So with this approximation $\overline{\vec{M}}$ becomes:

$$\overline{\vec{M}} = \vec{\mu} + \int d\vec{r}\, \vec{P} = \frac{9\epsilon}{(\epsilon+2)(2\epsilon+1)}\vec{\mu} \tag{A.33}$$

At the end of this section we remark that it was necessary to first consider a finite region and finally take the limit to an infinite medium to avoid the infinities alluded to in previous sections.

B Kirkwood's derivation.

In this appendix we paraphrase Kirkwood's derivation of the reaction field, to show more clearly where the differences with Onsager are. For the larger part the derivation in the previous appendix can be used. The major change is that the central cavity is now made larger, so that eventually it has the same properties as the dielectric as a whole.
It seems to me that the expression Kirkwood derives is basically the same as (A.9) but with the dipole moment of the central dipole replaced by $\vec{M}(R, r_0)$, so that

$$\overline{\vec{M}} = \frac{9\epsilon}{(\epsilon+2)(2\epsilon+1)}\vec{M}(R, r_0) \tag{B.1}$$

and $\vec{M}(R, r_0)$ has the meaning of a dipole moment the central cavity has if it is large enough to have a dielectric constant equal to the dielectric constant of the medium as a whole.
Then Kirkwood argues that actually we may just take the central dipole with its first solvation shell, calculate the effective dipole moment of that, which means including the local structure.
In fact this entails taking some limits, so he defines the dipole moment in that limit as

$$\overline{\vec{\mu}} = \lim_{r_0\to\infty} \vec{M}(R, r_0) \tag{B.2}$$

so that he can write as a relation for the dielectric constant:

$$\overline{\vec{M}} = \frac{9\epsilon}{(\epsilon+2)(2\epsilon+1)}\overline{\vec{\mu}} \tag{B.3}$$

which then immediately yields eq. (8.10).

C Macroscopic and microscopic susceptibility.

In this appendix we discuss some work by Bedeaux *et. al.* [9, 10] which has some additional insights to offer on the second problem mentioned in the final section. It must be remarked, however, that these only treat non–polar media.

The method is based on the solutions of the full Maxwell equations, which, in $\vec{k}$ space can be written as:

$$\vec{E}(\vec{k},\omega) = \vec{E}_v(\vec{k},\omega) - \mathrm{F}(\vec{k},\omega)\cdot\vec{P}(\vec{k},\omega) \tag{C.1}$$

In this equation $\vec{E}_v(\vec{k},\omega)$ is the solution to the Maxwell equations in vacuum, and $\mathrm{F}(\vec{k},\omega)$ is the retarded propagator, given by:

$$\mathrm{F}(\vec{k},\omega) = \frac{\omega^2}{\epsilon_0 c^2}\left[\vec{k}\vec{k} - k^2 + \frac{(\omega+i0)^2}{c^2}\right]^{-1} = \frac{1}{\epsilon_0(k^2-(\omega+i0)^2/c^2)}\left[\vec{k}\vec{k} - \frac{\omega^2}{c^2}\right] \tag{C.2}$$

We put in an $i0$ to indicate that we give the frequency an infinitesimally small positive imaginary part, to insure we only get the retarded solution.

Derivation of the last equality.

We need the inverse of the tensor $\vec{k}\vec{k} - \alpha^2$:

$$\mathrm{T} = \left[\vec{k}\vec{k} - \alpha^2\right]^{-1} \tag{C.3}$$

To that end we multiply both members with $\vec{k}\vec{k} - \alpha^2$, to get

$$\mathrm{T}\cdot\left[\vec{k}\vec{k} - \alpha^2\right] = 1 \tag{C.4}$$

Multiplying on the right with respectively $\hat{k}\hat{k}$ and $1 - \hat{k}\hat{k}$ yields

$$\mathrm{T}\cdot\left[\vec{k}\vec{k} - \alpha^2\right]\cdot\hat{k}\hat{k} = \mathrm{T}\cdot\hat{k}\hat{k}(k^2-\alpha^2) = \hat{k}\hat{k} \tag{C.5}$$

and

$$\mathrm{T}\cdot\left[\vec{k}\vec{k} - \alpha^2\right]\cdot\left(1-\hat{k}\hat{k}\right) = -\alpha^2\mathrm{T}\cdot\left(1-\hat{k}\hat{k}\right) = \left(1-\hat{k}\hat{k}\right) \tag{C.6}$$

Thus we get for the "longitudinal" and "transverse" components of T:

$$\mathrm{T}\cdot\hat{k}\hat{k} = \frac{\hat{k}\hat{k}}{k^2-\alpha^2} \tag{C.7}$$

and

$$\mathrm{T}\cdot\left(1-\hat{k}\hat{k}\right) = -\frac{1-\hat{k}\hat{k}}{\alpha^2} \tag{C.8}$$

Adding these two expressions then gives upon some rearrangement:

$$\mathrm{T} = \frac{1}{\alpha^2(k^2-\alpha^2)}\left(\vec{k}\vec{k} - k^2 + \alpha^2\right) \tag{C.9}$$

which, with $\alpha^2 = k^2 - \omega^2/c^2$, becomes

$$\mathrm{T} = \frac{c^2}{\omega^2(k^2-\omega^2/c^2)}\left(\vec{k}\vec{k} - \omega^2/c^2\right) \tag{C.10}$$

This indeed leads to the final equality in (C.2).

The next step is to give a constitutive relation between the polarization and the electric field. The polarization is given by the sum of the molecular dipole moments (strictly speaking the expectation values of the molecular dipole operators):

$$\vec{P}(\vec{r},t) = \sum_{i=1}^{N} \vec{\mu}_i(t)\delta(\vec{r} - \vec{r}_i(t)) \tag{C.11}$$

The simplest one can think of is at the molecular level the following

$$\vec{\mu}_i(\omega) = \epsilon_0 \chi_i^M(\omega) \cdot \vec{E}(\vec{r}_i, \omega) \tag{C.12}$$

where $\chi_i^M(\omega)$ is the molecular susceptibility tensor of particle i. It obviously depends in general on the orientation of the molecule, hence the index i.
A simplification of this is studied by Bedeaux *et. al.*, where the molecular susceptibility is taken to be a scalar quantity, independent of the frequency. In that case the eq. (C.11) can be written as

$$\vec{P}(\vec{r},t) = \epsilon_0 \chi^M \sum_{i=1}^{N} \delta(\vec{r} - \vec{r}_i(t))\vec{E}(\vec{r},t) = \epsilon_0 \chi^M \rho(\vec{r},t)\vec{E}(\vec{r},t) \tag{C.13}$$

where $\rho(\vec{r},t)$ is the microscopic particle density.
In the $\vec{k},\omega$ representation this is not diagonal, but rather a convolution integral, but we can write it formally as

$$\vec{P}(\vec{k},\omega) = \epsilon_0 \chi^{\text{op}} \odot \vec{E}(\vec{k},\omega) \tag{C.14}$$

where we introduced the notation $\chi^{\text{op}}\odot$ to indicate that we have to deal here with an integral operator in $\vec{k}$–space. With this definition (C.1) can be written as

$$\vec{E}(\vec{k},\omega) = \vec{E}_v(\vec{k},\omega) - \epsilon_0 \text{F}(\vec{k},\omega) \cdot \chi^{\text{op}} \odot \vec{E}(\vec{k},\omega) \tag{C.15}$$

with the formal solution:

$$\vec{E}(\vec{k},\omega) = \left[1 + \epsilon_0 \text{F}(\vec{k},\omega) \cdot \chi^{\text{op}}\right]^{-1} \odot \vec{E}_v(\vec{k},\omega) \tag{C.16}$$

Averaging this expression yields the macroscopic electric field:

$$\left\langle \vec{E}(\vec{k},\omega) \right\rangle = \left\langle \left[1 + \epsilon_0 \text{F}(\vec{k},\omega) \cdot \chi^{\text{op}}\right]^{-1} \right\rangle \odot \vec{E}_v(\vec{k},\omega) \tag{C.17}$$

The macroscopic susceptibility $\chi(\vec{k},\omega)$ is defined by the relation

$$\left\langle \vec{P}(\vec{k},\omega) \right\rangle = \epsilon_0 \chi(\vec{k},\omega) \cdot \left\langle \vec{E}(\vec{k},\omega) \right\rangle = \epsilon_0 \chi(\vec{k},\omega) \cdot \left\langle \left[1 + \epsilon_0 \text{F}(\vec{k},\omega) \cdot \chi^{\text{op}}\right]^{-1} \right\rangle \odot \vec{E}_v(\vec{k},\omega) \tag{C.18}$$

Averaging (C.14) yields, after substitution of (C.17):

$$\left\langle \vec{P}(\vec{k},\omega) \right\rangle = \left\langle \epsilon_0 \chi^{\text{op}} \odot \vec{E}(\vec{k},\omega) \right\rangle = \left\langle \epsilon_0 \chi^{\text{op}} \odot \left[1 + \epsilon_0 \text{F}(\vec{k},\omega) \cdot \chi^{\text{op}}\right]^{-1} \right\rangle \odot \vec{E}_v(\vec{k},\omega) \tag{C.19}$$

Comparison of the previous two equations then gives an expression for the macroscopic susceptibility in terms of the microscopic, by eliminating the vacuum field.

We remark here that we can use the following operator identity, written here for an arbitrary operator A:

$$[1+A]^{-1} = 1 - A\,[1+A]^{-1} \tag{C.20}$$

to get

$$\left\langle \left[1 + \epsilon_0 \mathrm{F}(\vec{k},\omega)\cdot\chi^{\mathrm{op}}\right]^{-1}\right\rangle = 1 - \mathrm{F}(\vec{k},\omega)\cdot\left\langle \epsilon_0\chi^{\mathrm{op}} \odot \left[1 + \epsilon_0 \mathrm{F}(\vec{k},\omega)\cdot\chi^{\mathrm{op}}\right]^{-1}\right\rangle \tag{C.21}$$

So that in fact we only need to calculate one average.

Static fields in an equilibrium dielectric.

The previous derivation was completely general, and since in this set of notes we restrict ourselves mainly to dielectrics in equilibrium, we now specialize to the equilibrium dielectric in the presence of a static field. This means that the applied fields become constants in time, and all averages are now averages over an equilibrium ensemble of polarizable molecules. All time/frequency dependence can thus be neglected, and we get for $\mathrm{F}(\vec{k})$:

$$\mathrm{F}(\vec{k}) = \frac{\vec{k}\vec{k}}{\epsilon_0 k^2} \tag{C.22}$$

For a collection of spherical molecules with polarizability α, we find for the microscopic susceptibility (see also eq. (3.1):

$$\epsilon_0\chi^{\mathrm{op}}(\vec{r}) = \alpha\rho(\vec{r}) \tag{C.23}$$

A constant vacuum field can be represented in $\vec{k}$–space by:

$$\vec{E}_v(\vec{k}) = (2\pi)^3\vec{E}_v\delta(\vec{k}) \tag{C.24}$$

To calculate inverses of operators, and subsequent averages, we obviously have to make use of series expansions. For the first term in such an expansion we get:

$$\epsilon_0\chi^{\mathrm{op}} \odot \vec{E}_v(\vec{k}) = \epsilon_0 \int \frac{d\vec{k}'}{(2\pi)^3}\,\chi^{\mathrm{op}}(\vec{k}-\vec{k}')\vec{E}_v(\vec{k}') = \alpha\rho(\vec{k})\vec{E}_v \tag{C.25}$$

Upon averaging this becomes

$$\left\langle \vec{P}(\vec{k})\right\rangle = \epsilon_0\left\langle \chi^{\mathrm{op}} \odot \vec{E}_v(\vec{k})\right\rangle = (2\pi)^3\alpha\rho_0\vec{E}_v\delta(\vec{k}) \tag{C.26}$$

where ρ_0 is the equilibrium particle density.
Similarly we can expand (C.18) to lowest order, to get:

$$\left\langle \vec{P}(\vec{k})\right\rangle = \epsilon_0\chi(\vec{k})\left\langle 1 - \epsilon_0\mathrm{F}(\vec{k})\cdot\chi^{\mathrm{op}}\right\rangle \odot \vec{E}_v(\vec{k}) \tag{C.27}$$

Performing a similar calculation as the one leading to (C.24), we obtain as an intermediate result:

$$\left\langle \vec{P}(\vec{k}) \right\rangle = \epsilon_0 \chi(\vec{k})(2\pi)^3 \left[1 - \alpha\rho_0 \frac{\vec{k}\vec{k}}{\epsilon_0 k^2} \cdot \right] \vec{E}_v \delta(\vec{k}) \tag{C.28}$$

Transforming back to $\vec{r}$–space we get for (C.24) and (C.26) respectively:

$$\left\langle \vec{P} \right\rangle = \alpha\rho_0 \vec{E}_v \tag{C.29}$$

and

$$\left\langle \vec{P} \right\rangle = \epsilon_0 \chi \left(1 - \frac{\alpha\rho_0}{3\epsilon_0} \right) \vec{E}_v \tag{C.30}$$

Combining these last two results, and using $\chi = \epsilon - 1$, we again find the Clausius–Mosotti relation:

$$\frac{\epsilon - 1}{\epsilon + 2} = \frac{\alpha\rho_0}{3\epsilon_0} \tag{C.31}$$

We also note from eq. (C.28) that the internal field is given by the Lorentz field. So there must be a relation between the boundary conditions, and the introduction of correlations between the particles, which is something we would like to explore further.

The second order terms.

The next term in the expansion of (C.19) gives:

$$\epsilon_0^2 \chi^{\mathrm{op}} \odot \mathrm{F}(\vec{k}) \cdot \chi^{\mathrm{op}} \odot \vec{E}_v(\vec{k}) \tag{C.32}$$

The problem with these expressions is that we have to be careful with the interpretation. The difficulty is caused by the fact that the F–operator is diagonal in $\vec{k}$–space, whereas χ^{op} is diagonal in $\vec{r}$–space.
Written in $\vec{k}$–space the full expression becomes:

$$\epsilon_0 \int \frac{d\vec{k}'}{(2\pi)^3} \chi^{\mathrm{op}}(\vec{k} - \vec{k}') \cdot \frac{\vec{k}'\vec{k}'}{k'^2} \cdot \int \frac{d\vec{k}''}{(2\pi)^3} \chi^{\mathrm{op}}(\vec{k}' - \vec{k}'') \cdot \vec{E}_v(\vec{k}'') \tag{C.33}$$

Introduction of (C.21) and (C.22) then gives:

$$\frac{\alpha^2}{\epsilon_0} \int \frac{d\vec{k}'}{(2\pi)^3} \rho(\vec{k} - \vec{k}')\rho(\vec{k}') \frac{\vec{k}'\vec{k}'}{k'^2} \cdot \vec{E}_v \tag{C.34}$$

The next step is averaging. To that end we need to calculate

$$\left\langle \rho(\vec{k} - \vec{k}')\rho(\vec{k}') \right\rangle = \int d\vec{r} \int d\vec{r}' \, e^{-i(\vec{k}-\vec{k}')\cdot\vec{r}} e^{-i\vec{k}'\cdot\vec{r}'} \left\langle \rho(\vec{r})\rho(\vec{r}') \right\rangle \tag{C.35}$$

where

$$\left\langle \rho(\vec{r})\rho(\vec{r}') \right\rangle = \sum_{i,j=1}^{N} \left\langle \delta(\vec{r} - \vec{r}_i)\delta(\vec{r}' - \vec{r}_j) \right\rangle = \rho_0 \delta(\vec{r} - \vec{r}') + \sum_{i \neq j} \left\langle \delta(\vec{r} - \vec{r}_i)\delta(\vec{r}' - \vec{r}_j) \right\rangle \tag{C.36}$$

Introduction of the pair–correlation function $\rho^{(2)}$[11], then leads to:

$$\left\langle \rho(\vec{r})\rho(\vec{r}') \right\rangle = \rho_0 \delta(\vec{r} - \vec{r}') + \rho^{(2)}(\vec{r} - \vec{r}') \tag{C.37}$$

Remark.

Translational invariance is maintained here, but only because the externally applied field does not exert a force on the polarizable molecules. Of course there are now the interactions between the induced dipoles. This does not lead to breaking of the translational invariance though.

In the papers by Bedeaux *et.al.* a cut–off radius is introduced, which is something we do not appear to be needing at all, at least not for the first order term. See the following, however.

Introduction of this result into eq. (C.33) the gives:

$$\left\langle \rho(\vec{k}-\vec{k}')\rho(\vec{k}')\right\rangle = (2\pi)^3\left[\rho_0 + \rho^{(2)}(\vec{k}')\right]\delta(\vec{k}) \tag{C.38}$$

Now we do get a divergence, from the first term of this expression. This must somehow be related to the fact that an induced dipole produces an infinite field at its own position. Infinities like this are customarily avoided by introducing cavities, but somehow it seems to me that they should not occur at all, so maybe we can just leave out these terms? (see also Fixman [1], who appears to get only the $i \neq j$ terms).
So let's for the moment subtract this infinite self energy term, and proceed to calculate the polarization field. The remainder of the calculation is then relatively trivial. For the polarization in (C.19) we get (after back–transformation) up to this order:

$$\left\langle \vec{P}\right\rangle = \alpha\rho_0\vec{E}_v - \frac{\alpha^2}{\epsilon_0}\int \frac{d\vec{k}}{(2\pi)^3}\rho^{(2)}(\vec{k})\frac{\vec{k}\vec{k}}{k^2}\cdot\vec{E}_v \tag{C.39}$$

A similar calculation using the remark below (C.19) gives for (C.18)

$$\left\langle \vec{P}\right\rangle = \epsilon_0\chi\left[1 - \frac{1}{3\epsilon_0}\left(\alpha\rho_0\vec{E}_v - \frac{\alpha^2}{\epsilon_0}\int \frac{d\vec{k}}{(2\pi)^3}\rho^{(2)}(\vec{k})\frac{\vec{k}\vec{k}}{k^2}\cdot\vec{E}_v\right]\right) \tag{C.40}$$

which leads to the Clausius-Mosotti type expression:

$$\frac{\epsilon-1}{\epsilon+2} = \frac{\alpha\rho_0}{3\epsilon_0}\left(1 - \frac{\alpha}{\epsilon_0\rho_0}\int \frac{d\vec{k}}{(2\pi)^3}\rho^{(2)}(\vec{k})\frac{\vec{k}\vec{k}}{k^2}\right) \tag{C.41}$$

It is fairly easy to see that due to the operator identity (C.20), we will in fact get a series expansion for the Clausius–Mosotti relation involving higher and higher order correlation functions. See also Fixman [1], who gives a slightly different derivation of this result.

Neglecting correlations.

If we neglect correlations, we can replace the n–particle correlation functions $\rho^{(n)}$ by $(\rho_0)^n$ [11]. This then leads to the following series for the Clausius–Mosotti expression:

$$\frac{\epsilon-1}{\epsilon+2} = \frac{\alpha\rho_0}{3\epsilon_0}\left(1 + \frac{\alpha\rho_0}{3\epsilon_0}\right)^{-1} \tag{C.42}$$

We just note here that this is not equal to the Onsager result for high densities.

References

[1] M. Fixman. Molecular theory of light scattering. *J. Chem. Phys.*, 23:2074–2079, 1955.

[2] H. Fröhlich. *Theory of Dielectrics.* Clarendon Press, Oxford, second edition, 1986.

[3] P. Debye. Einige Resultate einer kinetischen Theorie der Isolatoren. *Physik. Z.*, 13:97–100, 1912.

[4] H.A. Lorentz. *The Theory of Electrons.* B. G. Teubner, Leipzig, 1909.

[5] L. Onsager. Electric moments of molecules in liquids. *J. Am. Chem. Soc.*, 58:1486–1493, 1936.

[6] J.G. Kirkwood. The dielectric polarization of polar liquids. *J. Chem. Phys.*, 7:911–919, 1939.

[7] R.H. Cole. Induced polarization and dielectric constant of polar liquids. *J. Chem. Phys.*, 27:33–35, 1957.

[8] J.H. van Vleck. The influence of dipole–dipole coupling on the specific heat and susceptibility of a paramagnetic salt. *J. Chem. Phys.*, 5:320–337, 1937.

[9] D. Bedeaux and P. Mazur. On the critical behavior of the dielectric constant for a nonpolar fluid. *Physica*, 67:23–54, 1973.

[10] D. Bedeaux, A.M. Albano, and P. Mazur. Boundary conditions and non–equilibrium thermodynamics. *Physica*, 82A:438–462, 1976.

[11] J.–P. Hansen and I.R. McDonald. *Theory of Simple Liquids.* Academic Press, London, 1990.

[12] C.J.F. Böttcher. Zur Theorie der inneren electrischen Feldstärke. *Physica*, 9:937–945, 1942.

[13] C.J.F. Böttcher. Die Druckabhängigkeit der Molekularpolarisation von dipolfreien Gasen und Flüssigkeiten. *Physica*, 9:945–639, 1942.

[14] A.D. Buckingham. Solvent effects in infra–red spectroscopy. *Proc. Roy. Soc.*, A 248:169–182, 1958.

[15] A.D. Buckingham. A theory of frequency, intensity and band–width changes due to solvents in infra–red spectroscopy. *Proc. Roy. Soc.*, A 255:32–39, 1960.

[16] A.J. Dekker. On the reaction field of an eccentric dipole. *Physica*, 12:209–216, 1946.

[17] A. Einstein. Theorie der Opaleszenz von homogenen Flüssigkeiten und Flüssigkeitsgemischen in der Nähe der kritischen Zustandes. *Ann. Phys.*, 33:1275–1298, 1910.

[18] H. Fröhlich. Dielectric polarization in polar substances. Remark on a paper by F.E. Harris and B.J. Alder. *J. Chem. Phys.*, 22:1804–1806, 1954.

[19] R.M. Fuoss. Influence of dipole fields between solute molecules. I. On osmotic properties. *J. Am. Chem. Soc.*, 56:1027–1030, 1934.

[20] R.M. Fuoss. Influence of dipole fields between solute molecules. II. On molecular polarization. *J. Am. Chem. Soc.*, 56:1031–1033, 1934.

[21] F.E. Harris and B.J. Alder. Dielectric polarization in polar substances. *J. Chem. Phys.*, 21:1031–1038, 1953.

[22] F.E. Harris and B.J. Alder. Statistical mechanical derivation of Onsager's equation for dielectric polarization. *J. Chem. Phys.*, 22, 1954.

[23] F.E. Harris. Contributions of fluctuations and anisotropy to dielectric polarization in polar substances. *J. Chem. Phys.*, 23:1663–1672, 1955.

[24] P. Madden and D. Kivelson. A consistent molecular treatment of dielectric phenomena. *Adv. Chem. Phys.*, 56:467–566, 1984.

[25] Th. G. Scholte. A contribution to the theory of the dielectric constant of polar liquids. *Physica*, 15:437–449, 1949.

[26] M. von Smoluchowski. Molekular–kinetische Theorie der Opaleszenz von Gases im kritischen Zustande, sowie einiger verwandter Erscheinungen. *Ann. Phys.*, 25:205–226, 1908.

[27] J.H. van Vleck. On the role of dipole–dipole coupling in dielectric media. *J. Chem. Phys.*, 5:556–568, 1937.

[28] B.H. Zimm. Molecular theory of the scattering of light in fluids. *J. Chem. Phys.*, 13:141–145, 1945.

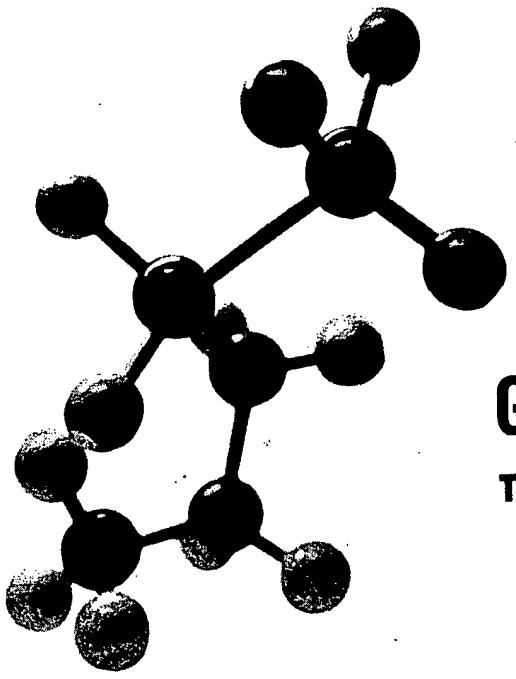

GENERAL

THIRD EDITION

HARPER & ROW, PUBLISHERS New York and London

ENERAL

IRD EDITION

v York and London

COLLEGE CHEMISTRY

CHARLES W. KEENAN
Professor of Chemistry
The University of Tennessee

JESSE H. WOOD
Professor of Chemistry
The University of Tennessee

LIBRARY OF CONGRESS CATALOG CARD NUMBER: 66-11267

Photographs appearing on the cover and title page are by James M. Cron.

tween solute and solvent molecules have hardly any effect in the formation of a solution in the gaseous state, because the particles are so widely separated.

WHY SUBSTANCES DISSOLVE

Although it is beyond the scope of this book to mention all factors involved in the formation of a solution, the ones of prime importance in forming liquid solutions are (1) interaction of solute and solvent to form solvated particles, (2) reaction of solute and solvent to form a new substance that becomes solvated, and (3) the tendency of systems to attain a maximum disorder.

Solvation. *Solvation* is the interaction of solvent molecules with solute molecules or ions to form aggregates whose particles are loosely bonded together. When water is used as the solvent, the process is also called aquation or hydration.

We saw in Chap. 5 that many covalent compounds are composed of polar molecules. Water is a familiar example. When a small crystal of an ionic substance such as sodium chloride is placed in water, the polar molecules orient themselves about the face of the crystal, as shown in Fig. 10-3. The attractive force between the water molecules

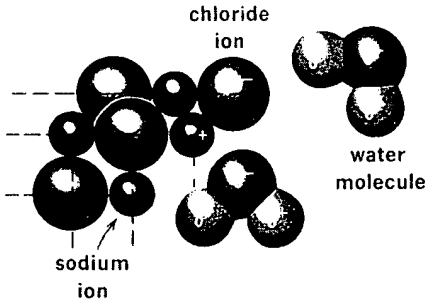

Polar water molecules and ions mutually attract each other.

FIG. 10-3

and the surface ions is great enough to cause the ions to leave their fixed positions in the crystal and to move to positions between the water molecules. Water molecules are actually loosely bonded to a sodium ion or a chloride ion in solution, as shown in Fig. 10-4. Both ions are said to be solvated or aquated.

Solvation is not limited to ionic compounds. Any polar covalent solute may interact with a polar solvent. Glucose sugar is a

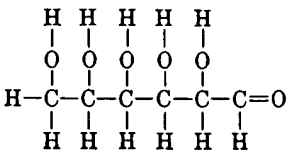

covalent compound with polar groups that dissolves in water because of solvation. Each hydroxyl group (—O—H) represents a